Seismicity and Faulting in the Southern Gulf of California

Danielle F. Sumy *(Lamont-Doherty Earth Observatory),* **James B. Gaherty** *(Lamont-Doherty Earth Observatory),* **Tobias Diehl** *(Lamont-Doherty Earth Observatory),* **Won-Young Kim** *(Lamont-Doherty Earth Observatory),* **John Collins** *(Woods-Hole Oceanographic Institution)*

The Sea of Cortez Ocean-Bottom Array (SCOOBA) seismic experiment consists of a 4-component broadband ocean-bottom seismic (OBS) array that recorded earthquakes and other natural seismic signals for nearly 12 months between October 2005 and October 2006. The 14-station array was designed to complement the onshore NARS-Baja experiment run by Utrecht University, Cal Tech, and CICESE. Two subarrays were centered within the Alarcon and Guaymas basins, coinciding with previous refraction and MCS lines [*Lizarralde et al., 2007*], with ~20 km spacing. Four additional instruments were deployed at ~100 km spacing. Over 650 earthquakes (depths < 35 km) were recorded by the array, with ~320 M>3.5 earthquakes and seven M>5 strike-slip events within the southern gulf that are accompanied by several foreshocks and aftershocks. Most of these events are located on the major NW-SE strike slip faults that delineate the plate boundary, but a few appear to be located on faults well away from the nominal plate boundary. For sufficiently well-recorded and paired events, we are in the process of applying the hypoDD double-difference algorithm to obtain high-precision relative relocations. Additionally, we are working towards modeling the Rayleigh waves of ~30 events to determine the mechanisms of on- and off-axis activity. These locations and mechanisms of earthquake activity will improve our understanding of the distribution of seismic deformation within the greater extensional zone in the southern GoC. These data have been archived at the IRIS DMC, and are openly available to the community.

References

Lizarralde, D., G. J. Axen, H. E. Brown, J. M. Fletcher, A. Gonzalez-Fernandez, A. J. Harding, W. S. Holbrook, G. M. Kent, P. Paramo, F. Sutherland and P. J. Umhoefe, Variation in the styles of rifting in the Gulf of California, *Nature, 448*, 466-469, 2007.

Acknowledgements: Funding is from the NSF MARGINS program, award number OCE 0436411 for James Gaherty at LDEO, and OCE 0305140 for John Collins at WHOI.

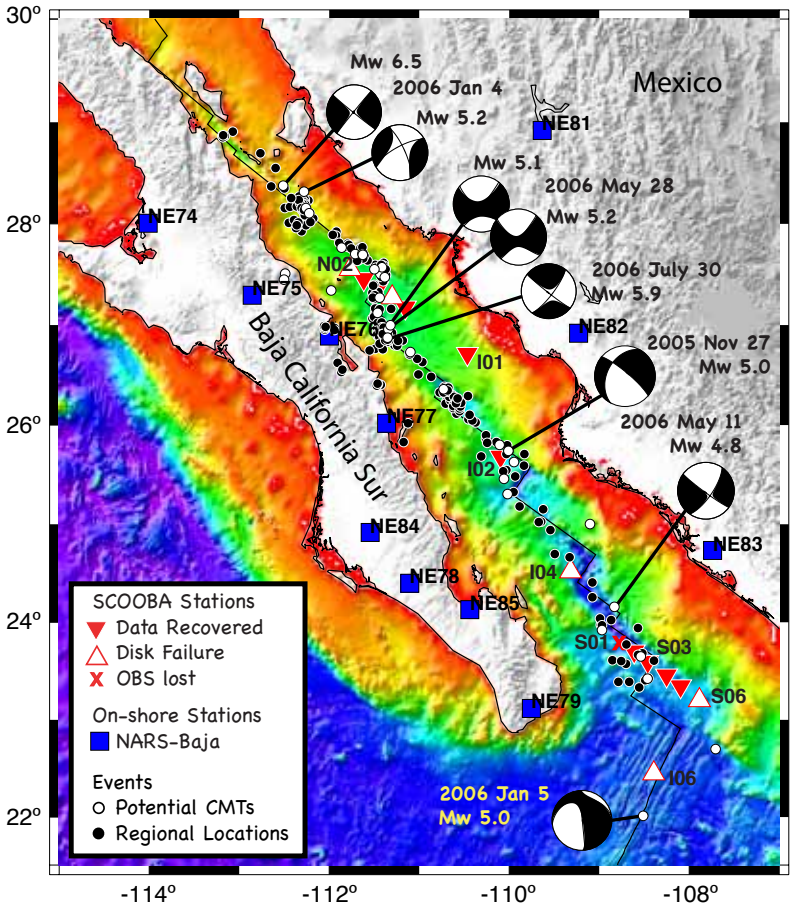

Figure 1. Location of the SCOOBA OBS stations (triangles), as well as complementary on-shore broadband NARS-Baja stations (blue squares). Also shown are Global CMT mechanisms for seven large events recorded by the array, our modeled mechanism for the 27 November 2005 event, and the locations for ~300 of our best-located events (black circles).

Local Earthquakes in the Dallas-Ft. Worth Region

Brian Stump *(Southern Methodist University),* **Cliff Frohlich** *(University of Texas at Austin),* **Chris Hayward** *(Southern Methodist University),* **Eric Potter** *(University of Texas at Austin)*

Injection or removal of fluids in the shallow crust can trigger earthquakes. In October 2008 and May 2009, small earthquakes occurred which were felt by numerous Dallas-Fort Worth (DFW) residents. PASSCAL provided six, three-component broad-band seismographs that were operated for two months following the October 2008 earthquakes. Preliminary analysis of these data and regional seismic data [*Frohlich et al., 2010*] demonstrates that: (1) Between 30 October 2008 and 31 December 2009, approximately 180 earthquakes occurred with probable hypocenters on or near DFW airport property; (2) Eleven of these were locatable by the local network and had hypocenters with focal depths of ~4.4 km situated along a 1.1 km SW-NE line near the south boundary of the DFW airport (Figure); (3) These hypocenters were situated approximately 500 m from a 4.2 km deep saltwater disposal (SWD) well where injection began on 12 September 2008, seven weeks before the first earthquake; (4) The hypocenters and the SWD well were situated near a mapped NE-SW trending subsurface fault, oriented such that slip along this fault was consistent with regional tectonic stresses; and (5) No evidence was found that drilling, hydrofracture, or natural gas production caused the earthquakes. The timing and proximity to the SWD well suggests that fluid injection at the SWD well may have induced the earthquakes. In June 2009, residents of Cleburne, TX, felt a second series of small earthquakes 60 miles south of DFW. Ten seismograph stations were deployed. Preliminary analysis of these data indicates that small earthquakes continued near Cleburne until at least November 2009, and that they also occurred near a SWD well. Following the felt earthquakes local and national news media called attention to the possible relationship between the earthquakes and the ongoing development of natural gas in the Fort Worth Basin. Even though the largest of the earthquakes had a magnitude of only M3.3, and they seemed unrelated to hydraulic fracturing, groups opposed to the development of tight gas shales considered them as evidence supporting their position. As noted in the Wall Street Journal, "the quake concerns come at a sensitive time for the industry, which is battling proposed legislation in Congress that would more heavily regulate hydraulic fracturing."

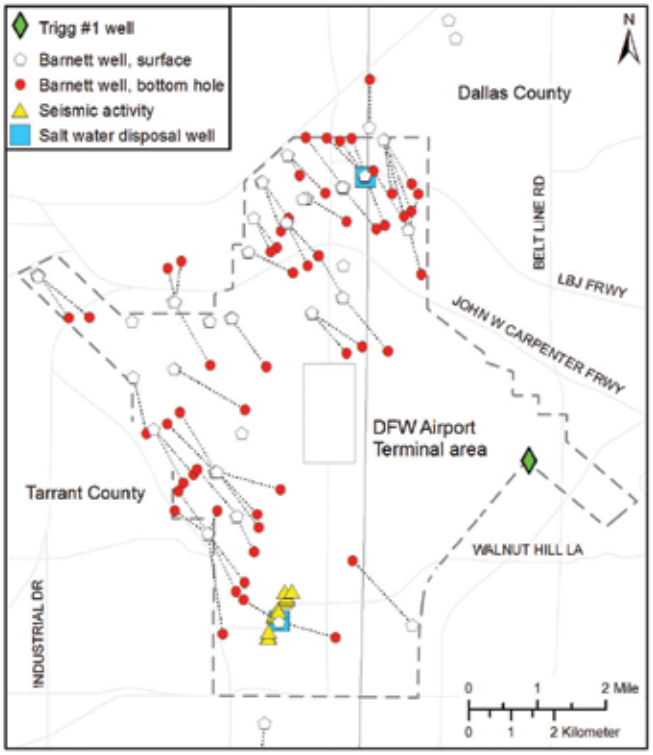

Map of DFW airport, showing location of earthquakes located by the temporary network (yellow triangles), tops and bottom of producing gas wells (white and red circles), and SWD wells (blue squares). The mean of the DFW earthquake location estimates using a linear velocity model is less than a kilometer from the bottom of the south SWD well.

References

Frohlich, C., E. Potter, C. Hayward, and B. Stump, Dallas-Fort Worth earthquakes coincident with activity associated with natural gas production, *Leading Edge, 29*, 270-275, 2010.

Use of ANSS Strong-Motion Data to Analyze Small Local Earthquakes

Kristine Pankow *(University of Utah Seismograph Stations),* **James Pechmann** *(University of Utah Seismograph Stations),* **Walter Arabasz** *(University of Utah Seismograph Stations)*

Traditionally, accelerometers have been used for recording triggered strong-ground motions from earthquakes with M > 4. The data from these instruments have been primarily used by engineers for building design and by seismologists modeling fault rupture histories. Although older generation strong-motion instruments were "incapable of recording small or distant earthquakes" (USGS, 1999, p. 12), advances in accelerometer and digital recording technology have greatly reduced this limitation. Following the 2002 Denali Fault earthquake we learned that modern continuously telemetered strong-motion instruments provide valuable recordings of some teleseismic earthquakes [Pankow et al., 2004]. Since then, we have learned that these instruments also provide valuable recordings of small (0.5 < M < 4) local earthquakes. Hundreds of modern strong-motion instruments have been deployed during the last decade as part of the U.S. Geological Survey Advanced National Seismic System (ANSS). Using the archive of continuous data from University-of-Utah-operated ANSS stations stored at the IRIS DMC, we determined the magnitude and distance ranges over which first arrivals could be successfully picked from accelerometers located on both rock and soil in northern Utah (see figure). The earthquake dataset consisted of 31 earthquakes (M 0.5 to M 3.2) located in the Salt Lake Valley. Somewhat surprisingly, earthquakes as small as M 2 are well-recorded on accelerometers to epicentral distances of 35 to 45 km at soil sites and 70 km at rock sites. ANSS accelerometers are collecting a rich new dataset, much of which is being archived at the IRIS DMC. This dataset is important not just for recording "the big one" and for strong-motion seismology, but also for studies of teleseisms, structure, and local seismicity.

References

Pankow, K.L., W.J. Arabasz , S.J. Nava, and J. C. Pechmann, Triggered seismicity in Utah from the 3 November 2002 Denali fault earthquake, *Bull. Seismol. Soc. Amer., 94*, S332-S347, 2004.

Pankow, K.L., J. C. Pechmann, and W.J. Arabasz , Use of ANSS strong-motion data to analyze small local earthquakes, *Seismol. Res. Lett., 78*, 369-374,2007.

USGS, An assessment of seismic monitoring in the United States: Requirement for an Advanced National Seismic System: U.S. Geological Survey Circular 1188, 55 p., 1999.

Acknowledgements: This project was supported by the U.S. Geological Survey, Department of the Interior, under USGS award number 04HQAG0014, and by the State of Utah under a line-item appropriation to the University of Utah Seismograph Stations.

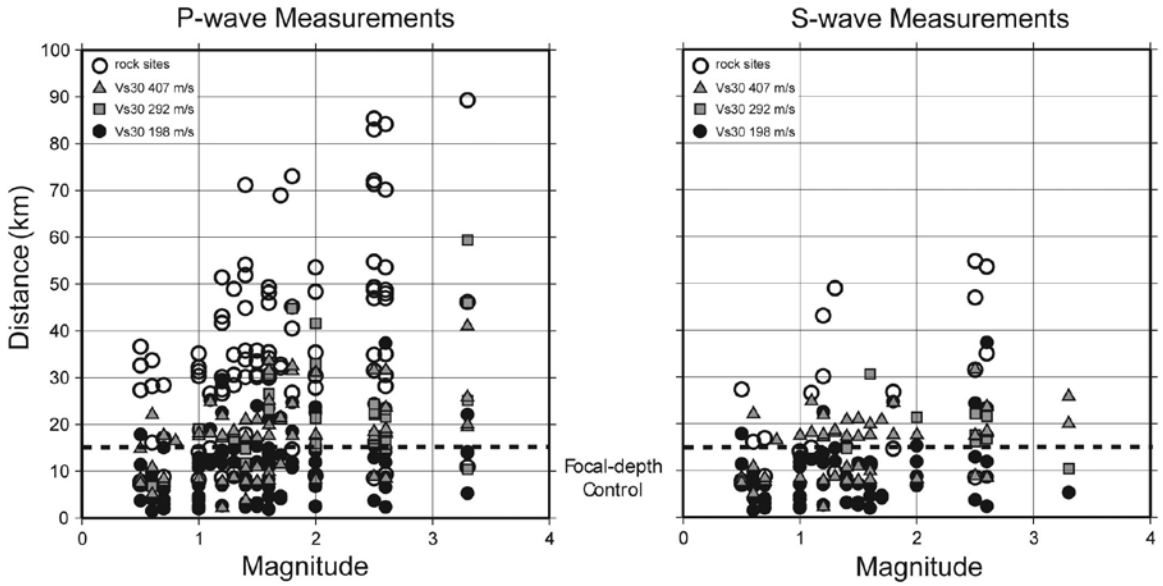

Plots (from Pankow et al., 2007) showing the distribution, as a function of distance, magnitude, and site response unit (see key) of all measurable arrival times for P-waves (left) and S-waves (right) recorded by accelerometers from 31 earthquakes in the western Salt Lake Valley. The dashed line at 15 km distance envelops those picks (< 15 km) that could improve focal-depth control.

Epicentral Location Based on Rayleigh Wave Empirical Green's Functions from Ambient Seismic Noise

Anatoli Levshin *(University of Colorado at Boulder),* **Michail Barmin** *(University of Colorado at Boulder),* **Michael Ritzwoller** *(University of Colorado at Boulder)*

A new method to locate the epicenter of regional seismic events is developed with strengths and limitations complementary to existing location methods. This new technique is based on applying Empirical Green's Functions (EGFs) for Rayleigh waves between 7 and 15 sec period that are determined by cross-correlation of ambient noise time-series recorded at pairs of seismic receivers. The important advantage of this method, in comparison with standard procedures based on use of body wave travel times, is that it does not employ an earth model. Rather it is based on interpolating the EGFs to arbitrary hypothetical event locations. The method is tested by locating well known "Ground Truth" crustal events in the western US as well as locating seismic stations using the principal of reciprocity. Data from the EarthScope/ USArray Transportable Array as well as regional networks were used for location. In these applications, location errors average less than 1 km, but are expected to vary with event mechanism and depth.

References

Barmin, M.P., A.L. Levshin, Y. Yang, and M.H. Ritzwoller, 2010. Epicentral Location Based on Rayleigh Wave Empirical Green's Functions from Ambient Seismic Noise. Submitted to *Geophys. J. Int.*

Acknowledgements: This research was supported by DoE/NNSA contract DE-AC52-09NA29326

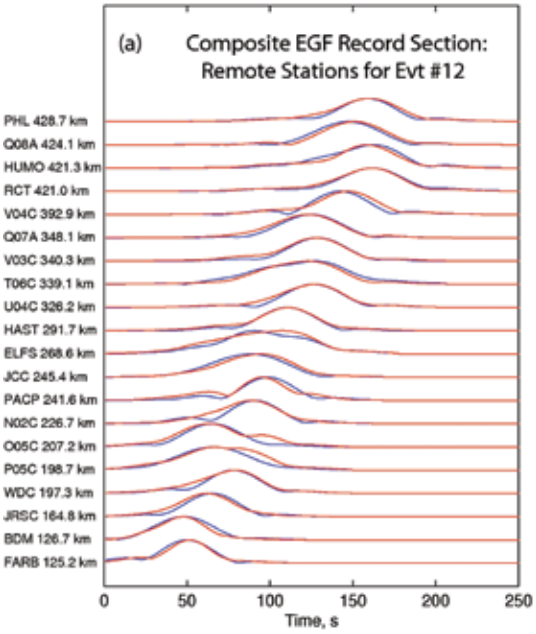

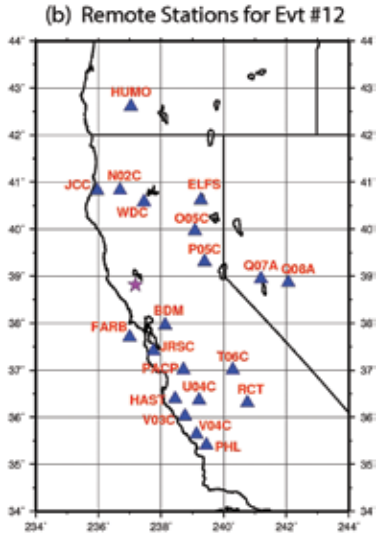

Record section of the Composite Empirical Green's Functions compared with the earthquake records at 20 remote stations for Event on in Northern California. (a) Envelope functions of the earthquake observed at the remote stations (red lines) are compared with envelopes of the Composite EGFs (blue lines). Band-pass: 7-15 sec period. Epicentral distances and station names are indicated at left. (b) Locations of the remote stations (blue triangles) and the earthquake (red star).

Schema of the Crandall Canyon mine. Our location of the event (green star) and corresponding 90% confidence ellipse. The left yellow push-pin marks the USGS event location, and the right push-pin is the approximate location of the mine collapse and trapped miners.

Rupture Fault Determination of the 2008 Mt. Carmel, Illinois, Earthquake in Wabash Valley Seismic Zone

Hongfeng Yang *(Saint Louis University),* **Lupei Zhu** *(Saint Louis University),* **Risheng Chu** *(Caltech)*

The April 18, 2008 Mt. Carmel Earthquake (magnitude 5.2) in southeastern Illinois underscores potential earthquake hazards in the Wabash Valley seismic zone. Since there was no surface rupture, the causal fault of the earthquake was not clear. In this study, we first developed a sliding-window cross-correlation (SCC) detection technique and detected more than 120 aftershocks in the two-week time window following the mainshock by applying the technique to continuous waveforms. We then precisely relocated 28 aftershocks out of all detected events by the double-difference relocation algorithm using accurate P- and S-wave differential arrival times between events obtained by waveform cross correlation. After relocation, we used the L1 norm to fit all located events by a plane to determine the mainshock fault plane. The best-fit plane has a strike of 292° and dips 81° to the northeast. By combining the aftershocks locations and focal mechanism solutions, we conclude that the April 18 earthquake occurred on a nearly vertical left-lateral strike-slip fault orienting in the WNW-ESE direction. The fault coincides with the proposed left-stepping Divide accommodation zone in the La Salle deformation belt and indicates reactivation of old deformation zone by contemporary stresses in the Midcontinent.

References

Yang, H., L. Zhu, and R. Chu, Fault-plane determination of the 18 April 2008 Mt. Carmel, Illinois, earthquake by detecting and relocating aftershocks, *Bull. Seismol. Soc. Amer., 99*(6), 3413-3420, 2009

Acknowledgements: This work is supported by NSF grant EAR-0609969. Waveform data are from the IRIS DMC.

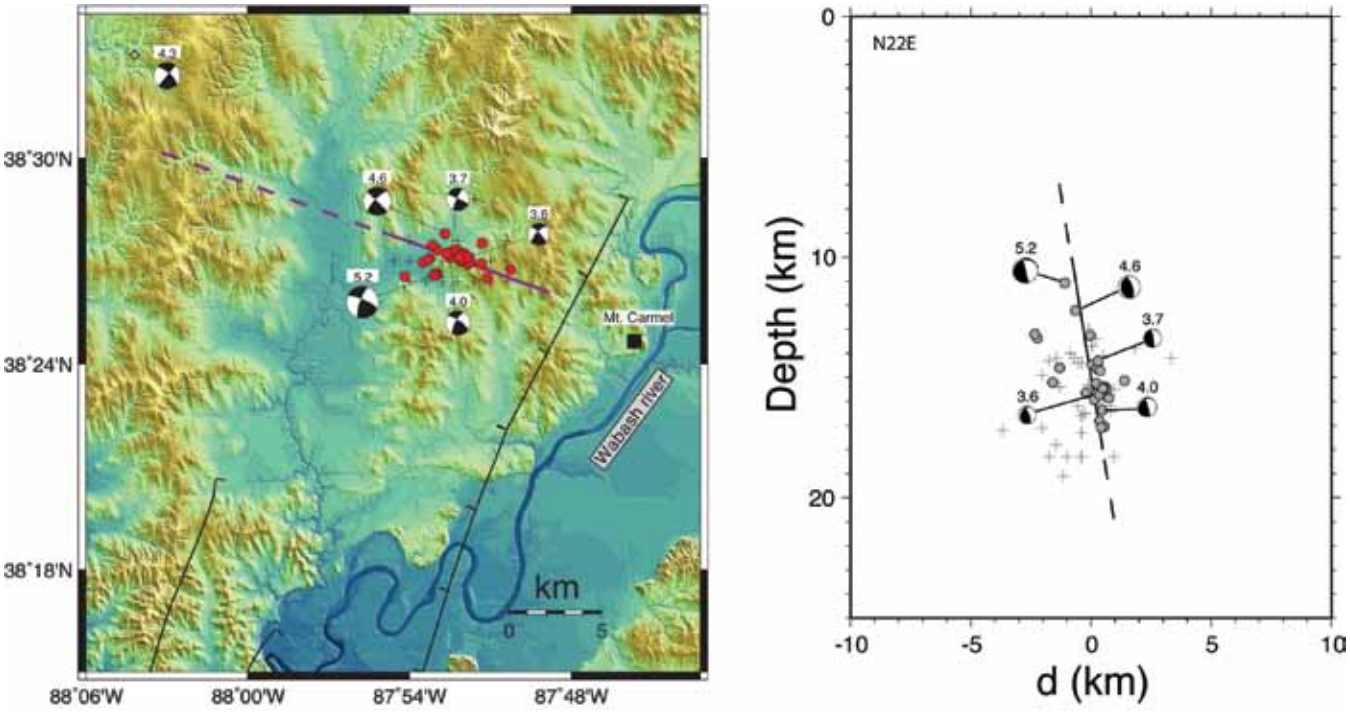

Map view (left) and vertical cross-section (right) of located aftershocks (red dots) of the 2008 Mt Carmel Earthquake. Their locations and earthquake focal mechanisms (beach balls) of the main-shock and four largest aftershocks suggest that the main-shock occurred on a nearly vertical fault orienting WNW-ENE (represented by the straight line).

Analysis of Spatial and Temporal Seismicity Patterns within Arizona During the Deployment of the EarthScope USArray Transportable Array (March 2006 - April 2009)

Jeffrey Lockridge *(Arizona State University),* **Matthew Fouch** *(Arizona State University),* **J. Ramon Arrowsmith** *(Arizona State University)*

Monitoring earthquake activity across the state of Arizona has historically been restricted by a paucity of regional seismic stations. Prior to 2006, earthquakes within Arizona were located at a rate of less than 30 events per year, presenting significant challenges for studies linking seismic activity and lithospheric strain accommodation. In this study, we utilize broadband seismic data recorded within Arizona by the EarthScope USArray Transportable Array (TA) (http://earthscope.org) to improve the characterization of the sources of tectonic strain accumulation and the mechanisms by which it is released. We built a Google Earth KMZ of global event data using EarthScope ANF monthly event archives to examine the spatial and temporal distribution of seismicity within Arizona during the deployment of the USArray TA. To date, we have identified 12 areas of seismicity within Arizona that exhibit event swarms with clear spatial and temporal correlations. We analyzed waveform data using the Antelope Environmental Data Collection Software package. We examined data from 8 TA stations nearest to each of 3 case studies and hand-picked P and S arrivals to generate a catalog of events for each swarm. We used a 1-5 Hz bandpass filter to detect events and a 0.3 Hz high-pass filter or no filter to pick arrivals. We present preliminary swarm characterization for these three case studies, which were chosen due to their distinctly different tectonic settings. (1) The linear-trending (NNE-SSW) Roosevelt Swarm is located within the Arizona Transition Zone and is adjacent to Roosevelt Lake, a ~35 km long reservoir on the Salt River with a maximum depth of ~100 m. (2) The spatially clustered Uinkaret Swarm is geologically located beneath the Uinkaret Volcanic Field on the north rim of the Grand Canyon (last known eruption ~1,100 years ago). The swarm is juxtaposed between 2 notable Quaternary faults (Hurricane and Toroweap) and is located within the Northern Arizona Seismic Belt along the western tectonic boundary of the Colorado Plateau. (3) The spatially clustered Shonto Swarm is geologically located within the Colorado Plateau. The nearest volcanic field is located ~47 km to the NE, and no known faults have been identified in the vicinity of this swarm.

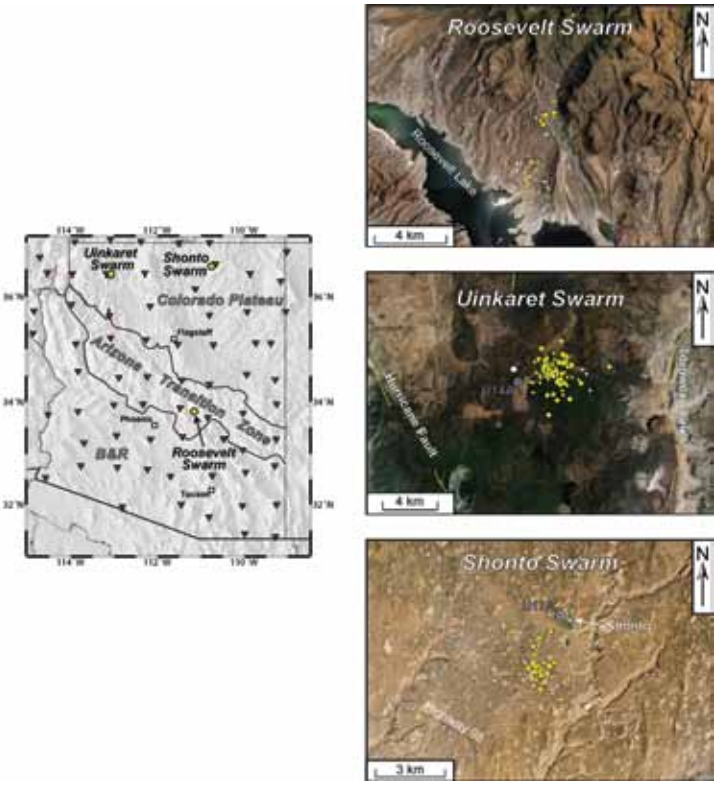

Figure Captions: Left: Locations of three earthquake swarms investigated as part of this study (yellow circles), USArray Transportable Array stations (red triangles), and the geologic/physiographic provinces of Arizona. Right Column: Google Earth screen captures of events from USArray ANF monthly archives (white circles), new events located as part of this study (yellow circles), and USArray TA stations (blue circles). Top Right: Roosevelt Swarm - 62 detections from 6/21/2007 to 6/28/2007 with 20 located events (3+ stations). Mag = 1.6 to 2.5 ml; Avg Depth = 3.8 km; Peak Activity = 10 events/hour. Middle Right: Uinkaret Swarm: 345 detections from 12/4/2007 to 12/17/2007 with 20 located events (3+ stations). Mag = 0.7 to 3.2 ml; Avg Depth = 13.5 km; Peak Activity = 18 events/hour. Bottom Right: Shonto Swarm: 172 detections from 8/29/2008 to 9/29/2008 with 34 located events (3+ stations). Mag = 0.8 to 2.8 ml; Avg Depth = 5.8 km; Peak Activity = 6 events/hour.

Acknowledgements: Acknowledgements: Financial support for this project came from U.S. National Science Foundation grant EAR-0548288 and the Federal Emergency Management Agency (FEMA). A huge thanks to the USArray Transportable Array team for installing and maintaining the stations used for this study. Waveform and Antelope database data were provided by Frank Vernon (USArray Array Network Facility) and the IRIS Data Management Center. Thanks also to the USArray Array Network Facility for a preliminary USArray event catalog. Historical Arizona earthquake database was provided by the Arizona Earthquake Information Center and the Arizona Integrated Seismic Network. Aerial photographs and Google Earth interface provided by Google.

Mozambique Earthquake Sequence of 2006: High-Angle Normal Faulting in Southern Africa

Z Yang *(Univ. of Colorado, Boulder),* **W.-P. Chen** *(Univ. of Illinois, Urbana)*

We report source mechanisms for the six largest shocks of the Mozambique earthquake sequence of 22 February 2006. The main shock of this sequence is one of the largest (Mw ~ 7.0) to occur in Africa over the past 100 years and its P waveforms alone are sufficient to show that north-south trending normal faulting near the surface continues to depths of more than 15 km along an exceptionally steep dip of 76° ± 4°. This new result shows that globally seismogenic normal faulting spans a wide range of dips, from about 30° to 75°. S waveforms, when combined with a minor component of left-lateral slip observed in the field, indicate the rake to be between −80° and −89° which, in turn, places a new constraint on relative plate motions: Complications from a nonspecific Rovuma microplate notwithstanding, our results favor the Euler pole between the Somalia and Nubia plates to lie southward of the epicenters.

Acknowledgements: We thank E. Calais, C. Collettini, C. Hartnady, R. Sibson, S. Stein, and Y. D. Zheng, for helpful discussions. In particular, S. Marshak suggested antithetic faulting in a listric master system. The data management centers of IRIS and GEOSCOPE kindly provided seismograms to us, and D. Doser, C.J. Ebinger, and B.W. Stump made careful reviews of the manuscript. This work is supported by the U.S. National Science Foundation grant EAR9909362 (Project Hi-CLIMB: An Integrated Study of the Himalayan-Tibetan Continental Lithosphere during Mountain Building, contribution I06). Any opinions, findings, and conclusions or recommendations expressed in this material are those of the authors and do not necessarily reflect those of the NSF.

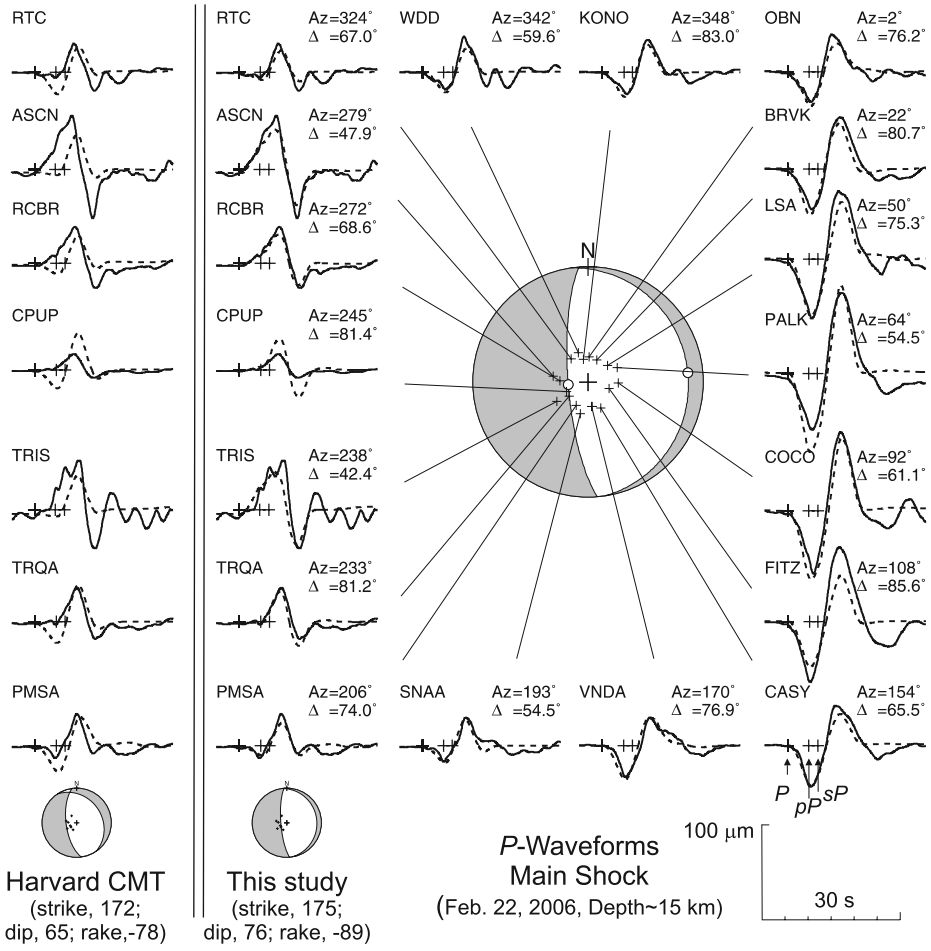

(right) Comparison between observed (solid traces) and synthetic P waveforms (dashed traces) of the main shock. The synthetic seismograms are calculated with a rupture history (source time function) represented by a symmetric triangle of 7.5 s in duration. Notice excellent azimuthal distribution of observations which are well matched by synthetic seismograms. (left) Comparison of synthetic seismograms based on the Harvard CMT solution with selected observations whose polarities of first motions are violated in several cases because a dip angle of 65° is too low. Open circles in the plot of fault plane solution are poles of nodal planes.

Exceptional Ground Motions from the April 26, 2008 Mogul Nevada Mw 5.0 Earthquake Recorded by PASSCAL Rapid Array Mobilization Program (RAMP) Stations

Glenn Biasi *(University of Nevada Reno),* **John G. Anderson** *(University of Nevada Reno),* **Kenneth D. Smith** *(University of Nevada Reno),* **Ileana Tibuleac** *(University of Nevada Reno),* **Rasool Anooshehpoor** *(University of Nevada Reno),* **David von Seggern** *(University of Nevada Reno)*

An unusually shallow swarm of earthquakes began 28 February 2008 beneath Mogul, Nevada, a small suburb a few km west of Reno. Earthquake depths of as shallow as 2 km were confirmed on instrumentation immediately over the hypocentral area, and residents routinely reported feeling events as small as Ml 1.5 or smaller. The swarm also exhibited an accelerating moment release over a period of several weeks. The slow build-up of the swarm allowed UNR to deploy four PASSCAL RAMP instruments in the epicentral area in early April 2008 to improve location control and map swarm evolution. Importantly, the RAMP stations included strong-motion sensors to ensure that any larger earthquakes would be recorded on scale.

Seismic activity accelerated throughout April, culminating in an Mw 5.0 mainshock at 06:40 UTC 26 April 2008 [*Anderson et al., 2009*]. Two stations immediately above the mainshock recorded component accelerations over 800 cm/s^2. Mean horizontal accelerations exceed 0.6 g at three of the four stations. The strongest peak acceleration was 1,164 cm/s^2, or about 1.19 g, at station MOGL, about 0.4 km from the epicenter. The peak vector velocity at MOGL was 54 cm/s, at a frequency of about 3 Hz. These accelerations far exceed design ground motions for the residential construction of the community, but nevertheless, damage to wood-frame buildings there was minimal. Ground motions also far exceeded predictions from the major ground motion regression equations, apparently because of the shallow hypocentral depth of about 3 km. At the same time, attenuation of peak ground motions was greater than predictions, suggesting that source-side attenuation was greater than for earthquakes with a more typical depth of 5-10 km. Peak accelerations and velocities from this earthquake would place it in the top 25 strongest ground motions ever recorded [*Anderson, 2010*]. These amazing recordings and new insights into shallow earthquake swarms would have remained unknown without timely access to PASSCAL RAMP instruments.

References

Anderson, J. G., I. Tibuleac, A. Anooshehpoor, G. Biasi, K. Smith, and D. von Seggern (2009). Exceptional ground motions recorded during the April 26, 2008 Mw 5.0 earthquake in Mogul, Nevada, *Bull. Seismol. Soc. Amer., 99*, 3475-3486.

Anderson, J. G. (2010). Source and site characteristics of earthquakes that have caused exceptional ground accelerations and velocities, *Bull. Seismol. Soc. Amer., 100*, 1-36.

Acknowledgements: The permanent network in western Nevada and easternmost California was supported by the United States Geological Survey under Cooperative Agreement 07HQAG0015.

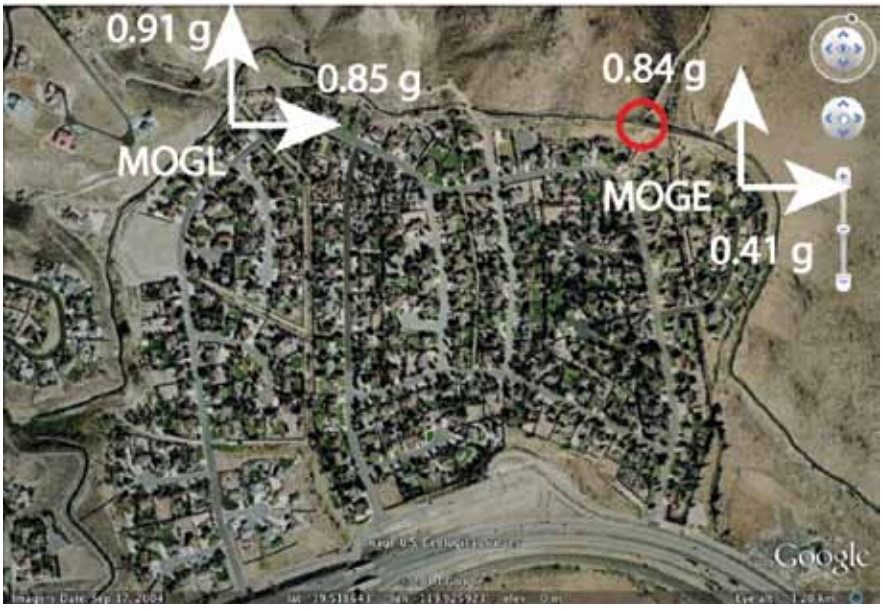

Mogul, Nevada community (Google Earth; center 39.5186, -119.9262; ~1.5 km N-S photo extent), with component ground accelerations measured from PASSCAL RAMP stations MOGL and MOGE. April 26, 2008 Mw 5.0 mainshock epicenter is indicated by the red circle.

Detailing a Shallow Crustal Earthquake Swarm beneath the Mogul, Nevada with PASSCAL RAMP Instrumentation

Glenn Biasi, Kenneth D. Smith, John G. Anderson *(University of Nevada, Reno)*

An anomalous swarm of shallow earthquakes began on 28 February 2008 beneath the suburban communities of Mogul and Somersett, Nevada, about 12 km west of downtown Reno. Initially the swarm consisted of a few earthquakes per week, but accelerated during March 2008 to include several felt events per day. Residents routinely reported feeling earthquakes of Ml 1.5 or smaller. Earthquake depths as shallow as 2 km were confirmed by a short-period station in the epicentral region. The relatively slow onset and sustained activity of the swarm provided time to request seismic instruments from the PASSCAL Rapid Array Mobilization Program (RAMP) pool. Four RAMP stations with broadband and strong-motion sensors were deployed in the epicentral area by 9 April 2008. The swarm began to accelerate in earnest in early April, with four Ml 3 or greater earthquakes on 15 April, two Ml 4 events on 24 April, and what proved to be the mainshock, an Mw 5.0 earthquake at 06:40 on 26 April 2008. This earthquake produced component ground accelerations in excess of 0.8 g at two stations, and horizontal vector accelerations in excess of 1.1 g at one station [*Anderson et al., 2009*]. These ground motions caused widespread non-structural and content damage to residences in the area.

Because of the social impact of the swarm and its potential to continue or even grow, six RAMP instruments deployed in central Nevada were relocated in early May to the epicentral area. An innovation in this deployment is that the RAMP stations were integrated by IP radio telemetry, beginning in late April 2008 into the permanent seismic monitoring network of the region operated by the University of Nevada Reno (UNR) (Figure 1). Antelope processing software at UNR allowed RAMP stations to be integrated seamlessly into the main network. This provided UNR personnel with highest-quality real-time information as the swarm evolved.

The Mogul swarm continued at a high level of daily activity through June 2008, and did not return to an activity rate similar to its first week until mid-August. Double-difference hypocentral relocations (Figure 2) identify a NW-trending vertical structure, consistent with the mainshock and focal mechanisms, with a smaller NE-trending spur toward the north end of the rupture zone. The Mogul swarm did not occur on any known or suspected fault and geologic investigation has not identified any surface expression or structure. Continuous GPS data gathered with the event resolved motions up to 2.5 cm at the surface, but indicate a geodetic moment release approximately twice as large as would be expected from the seismicity.

The Mogul sequence was the subject of a one-hour documentary by the National Geographic organization Naked Science series and aired by national cable-TV providers. Information is available at http://channel.nationalgeographic.com/series/naked-science/4232/Videos#tab-Overview.

References

Anderson, J. G., I. Tibuleac, A. Anooshehpoor, G. Biasi, K. Smith, and D. von Seggern (2009). Exceptional ground motions recorded during the April 26, 2008 Mw 5.0 earthquake in Mogul, Nevada, *Bull. Seismol. Soc. Amer., 99*, 3475-3486.

Acknowledgements: The permanent network in western Nevada and easternmost California was supported by the United States Geological Survey under Cooperative Agreement 07HQAG0015.

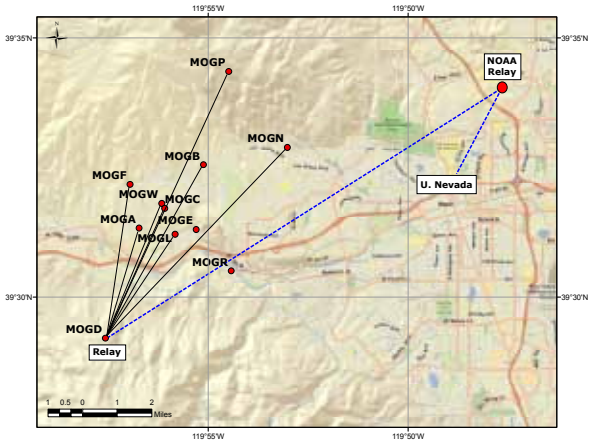

igure 1. PASSCAL RAMP stations and telemetry paths for the Mogul, Nevada earthquake swarm of 2008. Station MOGE used a cell modem, and station MOGR could not be telemetered by radio or cell because of line-of-sight issues. Seismic data was relayed to UNR and integrated into regional seismic network operations in real time.

Figure 2. Double-difference relocated earthquakes of the Mogul, Nevada earthquake swarm. The mainshock had an Mw of 5.0, but a local magnitude Ml 4.7. The mainshock hypocenter was approximately 3 km depth. Hypocenters do not coincide with any known fault or geologic structure. Downtown Reno, Nevada is near the east edge of the image.

The 2010 Mw7.2 El Mayor-Cucapah Earthquake Sequence, Baja California, Mexico and Southernmost California, USA: Active Seismotectonics along the Mexican Pacific Margin

Egill Hauksson *(Caltech, Seismological Laboratory),* **Joann Stock** *(Caltech, Seismological Laboratory),* **Kate Hutton** *(Caltech, Seismological Laboratory),* **Wenzheng Yang** *(Caltech, Seismological Laboratory),* **Antonio Vidal** *(CICESE, Mexico),* **Hiroo Kanamori** *(Caltech, Seismological Laboratory)*

The El Mayor-Cucapah earthquake sequence started with preshocks in March 2010, and a sequence of 15 foreshocks of M>2 (up to M4.4) that occurred during the 24 hours preceding the mainshock. The foreshocks occurred along a north-south trend near the mainshock epicenter. The Mw7.2 mainshock that occurred on the 4th of April exhibited complex faulting, possibly starting with a ~M6 normal faulting event, followed ~15 sec later by the main event, which included simultaneous normal and right-lateral strike-slip faulting. The aftershock zone extends for 120 km from the south end of the Elsinore fault zone at the US-Mexico border almost to the northern tip of the Gulf of California. The waveform-relocated aftershocks form two abutting clusters, of about equal length of 50 km each, as well as a 10 km north-south aftershock zone just north of the epicenter of the mainshock. Even though the Baja California data are included, the magnitude of completeness and the hypocentral errors increase gradually with distance to the south of the international border. The spatial distribution of large aftershocks is asymmetric with five M5+ aftershocks located to the south of the mainshock, and only one M5.7 aftershock but numerous smaller aftershocks to the north. Further, the northwest aftershock cluster exhibits complex faulting on both northwest and northeast planes. Thus the aftershocks also express a complex pattern of stress release along strike. The overall rate of decay of the aftershocks is similar to the rate of decay of a generic California aftershock sequence. In addition, some triggered seismicity was recorded along the Elsinore and San Jacinto faults to the north but significant northward migration of aftershocks has not occurred. The synthesis of the El Mayor-Cucapah sequence reveals transtensional regional tectonics, including the westward growth of the Mexicali Valley as well as how Pacific North America plate motion is transferred from the Gulf of California in the south into the southernmost San Andreas fault system to the north.

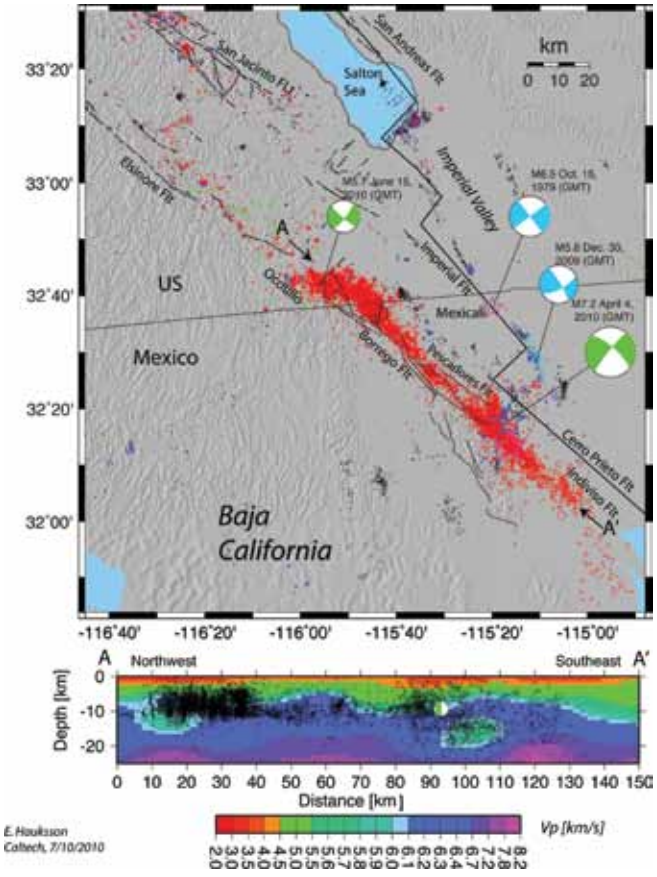

Map of the relocated hypocenters of foreshocks, mainshock, and aftershocks and 2009 background seismicity. The mainshock epicenter is indicated by a star. Foreshocks are shown as blue open circles beneath the mainshock star. The locations of the Vp cross section are indicated by the A-A' (includes focal mechanism of mainshock).

References

Hauksson, E., J. Stock, K. Hutton, W. Yang, A. Vidal, and H. Kanamori, The 2010 Mw7.2 El Mayor-Cucapah Earthquake Sequence, Baja California, Mexico and Southernmost California, USA: Active Seismotectonics Along the Mexican Pacific Margin, Submitted to *Pure Appl. Geophys.* Topical Issue: Geodynamics of the Mexican Pacific Margin, 10 July 2010

Acknowledgements: This research was supported by the USGS, SCEC, and CICESE.

Along-strike Variations in Shallow Earthquake Distribution and Source Parameters along the Kurile-Kamchatka Arc

Susan L. Bilek *(Earth and Environ. Science Dept., New Mexico Tech),* **Heather R. DeShon** *(CERI, University of Memphis),* **E. Robert Engdahl** *(Dept. of Physics, Univ. of Colorado)*

Observations in the last decade suggest a spectrum of slip durations for subduction zone earthquakes arising from rupture velocities that range from typical ~3 km/s, to 1 km/s for tsunami earthquakes, and even slower for other slip events. In order to understand conditions required to produce these slow rupture velocities, it is useful to clearly define areas where slow earthquakes occur. Our project addresses this goal by a) determining source parameters for large catalogs of subduction zone earthquakes, with an initial focus in expanding catalogs near documented tsunami earthquakes, and b) improving locations of these earthquakes to define regions of the interface that produce slow slip events through a new methodology that improves on the relocation technique of Engdahl, van der Hilst, and Buland (EHB). We show here results for 119 thrust mechanism earthquakes near the plate interface in the Kurile-Kamchatka subduction zone, an area with 2 documented tsunami events in 1963 and 1975 and afterslip following large coseismic slip. We determine a variety of earthquake source parameters using IRIS waveform data in multi-station body wave deconvolution methods and finite fault waveform inversion. Using the revised locations and their moment-normalized source durations, we find patches of events with long rupture durations around the 1963 tsunami event, along central Kuriles, and in southern Kamchatka, south of observed afterslip in 1997 (Figure 1).

References

Bilek, S.L., H.R. DeShon, and E.R. Engdahl, 2009, Along-Strike Variations in Shallow Earthquake Distribution and Source Parameters Along the Kurile-Kamchatka Arc, EOS Trans AGU, 90(52), Fall Meet. Suppl., Abstract T23B-1908

Acknowledgements: We gratefully acknowledge NSF-OCE support for this project (OCE-0840908 to SLB, OCE-0841022 to HRD, and OCE-0841040 to ERE.

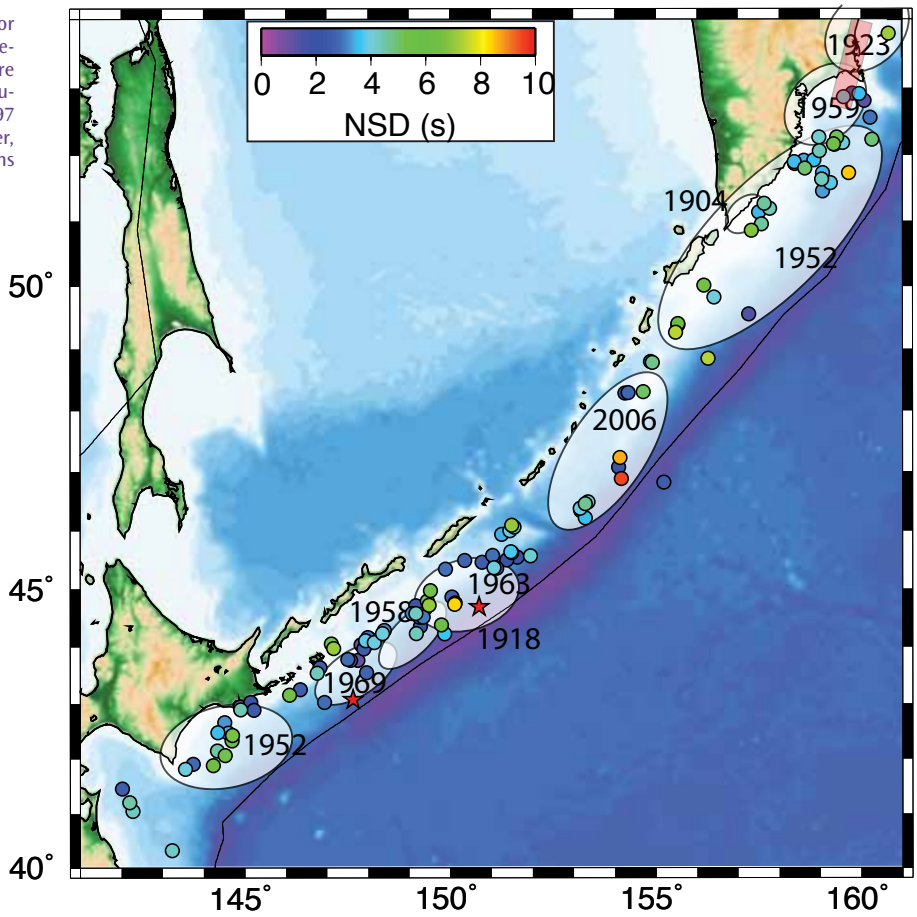

Moment normalized rupture duration (NSD) for earthquakes with revised locations along the Kurile-Kamchatka subduction zone. Our results suggest more recent earthquakes that occurred near the 1963 tsunami earthquake (red star) and south of the 1997 afterslip (red rectangle) have long duration character, suggesting the possibility of similar fault conditions leading to both slip processes.

Effects of Kinematic Constraints on Teleseismic Finite-Source Rupture Inversions: Great Peruvian Earthquakes of 23 June 2001 and 15 August 2007

Thorne Lay *(Univ. California, Santa Cruz),* **Charles J. Ammon** *(The Pennsylvania State University),* **Alexander R. Hutko** *(US Geological Survey),* **Hiroo Kanamori** *(California Institute of Technology)*

The rupture processes of two great under-thrusting earthquakes along the coast of Peru in 2001 and 2007 involve slip distributions that are distinctive from the predominantly unilateral or bilateral rupture expansion of many great events. Commonly used finite-source rupture model inversion parameterizations, with specified rupture velocity and/or short duration of slip at each grid point, applied to the seismic recordings for these two events lead to incorrect slip-distributions or inaccurate estimation of rupture velocities as a result of intrinsic kinematic constraints imposed on the model slip distributions. Guided by large aperture array back-projections of teleseismic broadband P-wave signals that image slip locations without imposing a priori kinematic constraints on the rupture process, we exploit the availability of large global broadband body and surface wave data sets to consider the effects of varying the kinematic constraints in teleseismic finite-source waveform inversions. By allowing longer than usual rupture durations at each point on the fault using a flexible subfault source time function parameterization, we find that the anomalous attributes of the 2001 and 2007 Peru earthquake ruptures are readily recognized and accounted for by compound rupture models. The great 23 June 2001 (Mw = 8.4) earthquake involved an initial modest-size event that appears to have triggered a much larger secondary event about 120 km away that developed an overall slip distribution with significant slip located back along the megathrust in the vicinity of the initial rupture. The great 15 August 2007 (Mw = 8.0) earthquake was also a composite event, with a modest size initial rupture followed by a 60 sec delayed larger rupture that initiated ~50-60 km away and spread up-dip and bilaterally. When back-projections indicate greater rupture complexity than captured in simple slip-pulse-type rupture model, one should allow for possible long-subfault-slip-duration or composite triggered sequences, and not overly constrain the earthquake slip distribution.

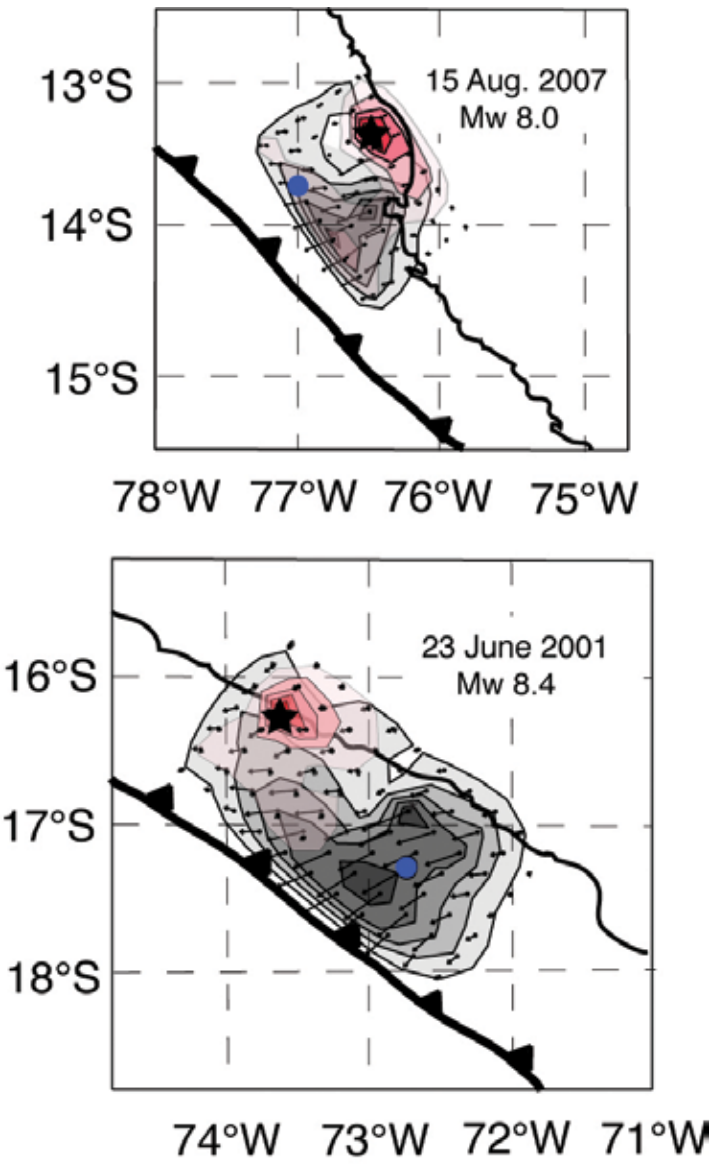

Maps showing the slip distribution for the preferred doublet event models for the 2007 (top) and 2001 (bottom) Peru earthquakes. The slip region for the first event in each pair is indicated by the orange tones. The stars indicate the USGS epicenters and the blue circles indicate the CMT centroid.

Acknowledgements: Supported by NSF grants EAR0453884 and EAR0635570 (TL) and USGS Award Number 05HQGR0174 (CJA).

The 2006-2007 Kuril Islands Great Earthquake Sequence

Thorne Lay *(Department of Earth and Planetary Sciences, Univ. California Santa Cruz),* **Hiroo Kanamori** *(Seismological Laboratory, California Institute of Technology),* **Charles J. Ammon** *(Department of Geosciences, The Pennsylvania State University),* **Alexander R. Hutko** *(U.S. Geological Survey),* **Kevin Furlong** *(Department of Geosciences, The Pennsylvania State University),* **Luis Rivera** *(Institut de Physique du Globe de Strasbourg)*

The southwestern half of a ~500-km-long seismic gap in the central Kuril Island arc subduction zone experienced two great earthquakes with extensive pre-shock and aftershock sequences in late 2006 to early 2007. The nature of seismic coupling in the gap had been uncertain due to the limited historical record of prior large events and the presence of distinctive upper plate, trench and outer-rise structures relative to adjacent regions along the arc that have experienced repeated great interplate earthquakes in the last few centuries. The intraplate region seaward of the seismic gap had several shallow compressional events during the preceding decades (notably an Ms 7.2 event on 16 March 1963), leading to speculation that the interplate fault was seismically coupled. This issue was partly resolved by failure of the shallow portion of the interplate megathrust in an Mw = 8.3 thrust event on 15 November 2006. This event ruptured ~250 km along the seismic gap, just northeast of the great 1963 Kuril Island (Mw = 8.5) earthquake rupture zone. Within minutes of the thrust event, intense earthquake activity commenced beneath the outer wall of the trench seaward of the interplate rupture, with the larger events having normal-faulting mechanisms. An unusual double band of interplate and intraplate aftershocks developed. On 13 January 2007, an Mw = 8.1 extensional earthquake ruptured within the Pacific plate beneath the seaward edge of the Kuril trench. This event is the third largest normal-faulting earthquake seaward of a subduction zone on record, and its rupture zone extended to at least 33 km depth and paralleled most of the length of the 2006 rupture. The great event aftershock sequences were dominated by thrust faulting for the 2006 rupture zone, and normal faulting for the 2007 rupture zone. A large intraplate compressional event occurred on 15 January 2009 (Mw = 7.4) near 45 km depth, below the rupture zone of the 2007 event and in the vicinity of the 16 March 1963 compressional event. The fault geometry, rupture process and slip distributions of the two great events are estimated using very broadband teleseismic body and surface wave observations. This great earthquake doublet demonstrates the heightened seismic hazard posed by induced intraplate faulting following large interplate thrust events. Future seismic failure of the northeastern region that has also experienced compressional activity seaward of the megathrust warrants particular attention.

References

Lay, T., H. Kanamori, C. J. Ammon, A. R. Hutko, K. Furlong, and L. Rivera (2009). The 2006-2007 Kuril Islands great earthquake sequence, *J. Geophys. Res., 114*, B113208, doi:10.1029/2008JB006280.

Acknowledgements: Supported by NSF grants EAR0453884 and EAR0635570 (TL) and USGS Award Number 05HQGR0174 (CJA).

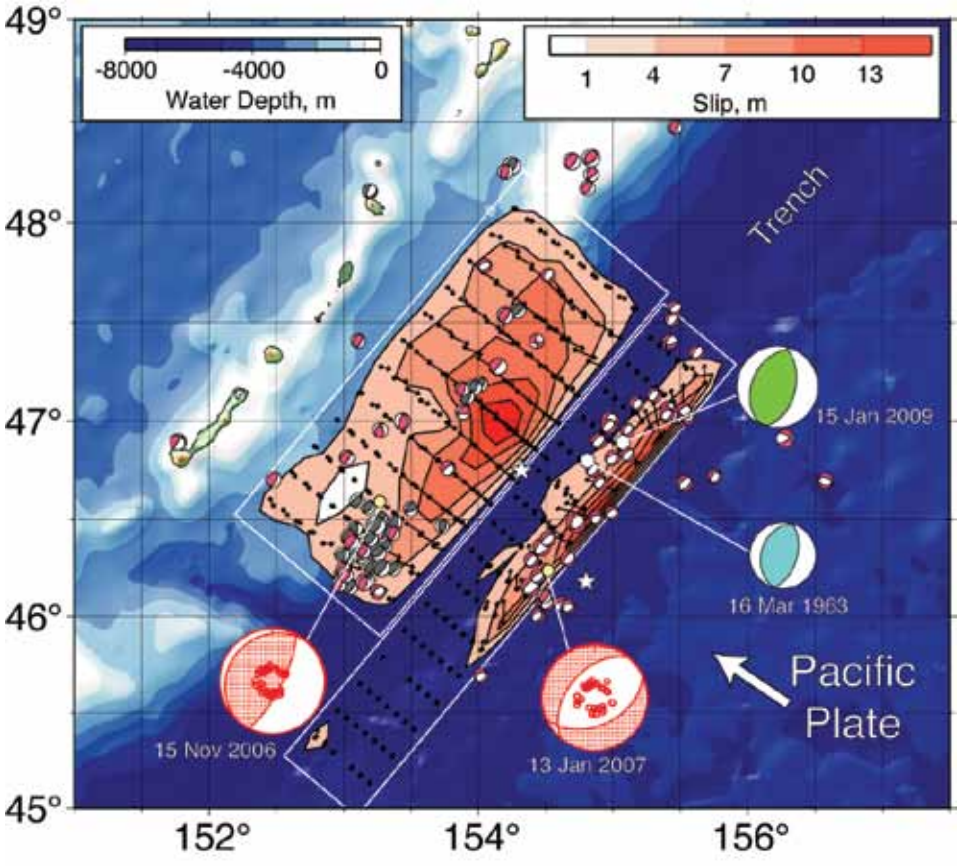

Surface map projection of coseismic slip for the 15 November 2006 (average slip 7.0 m) and the northwest dipping plane for 13 January 2007 (average slip 6.7 m at depths less than 25 km) events (NEIC epicenters: yellow circles, CMT centroid epicenters: stars).

Imaging of the Source Properties of the February 27, 2010, Maule, Chile Earthquake Using Data from the Transportable Array

Eric Kiser *(Harvard University),* **Miaki Ishii** *(Harvard University)*

The availability of high-quality data from a large, dense network of seismic stations achieved by the Transportable Array component of the USArray project has proven fruitful in studies of the subsurface structure. These data also provide vital information for imaging some of the rupture properties of giant earthquakes. The coherent arrivals throughout the array, combined with time-reversal to potential source locations, converts rich information of the waveform of a particular seismic phase to rupture propagation and relative energy release. This back-projection approach requires minimal a priori knowledge of the event, and with near real-time data, such as those from the Transportable Array, the analysis can be performed within the time window relevant for hazard mitigation, especially for tsunami assessment. The figure below shows an example of the application of the technique to the Maule, Chile earthquake that occurred on February 27, 2010 (Mw8.8). The Transportable Array was at a teleseismic distance for an effective P-wave back-projection. The large size of the array provided the necessary range in distance and azimuth for high resolution of the rupture process, and some details of the event are imaged with little artifacts. The rupture propagates primarily to the north from the epicentre for a length of 360 km and lasts about 120 seconds, corresponding to a rupture velocity of about 3.0 km/s. There is also a lower amplitude (relative to northern rupture) signal imaged to the south of the epicentre which reaches its maximum level at about 80 seconds after the event initiation. The images suggest a bilateral nature of the earthquake, and that the potential slip distribution is far from uniform, with main energy release located north of the epicentre occurring in the later part of the 120-second duration.

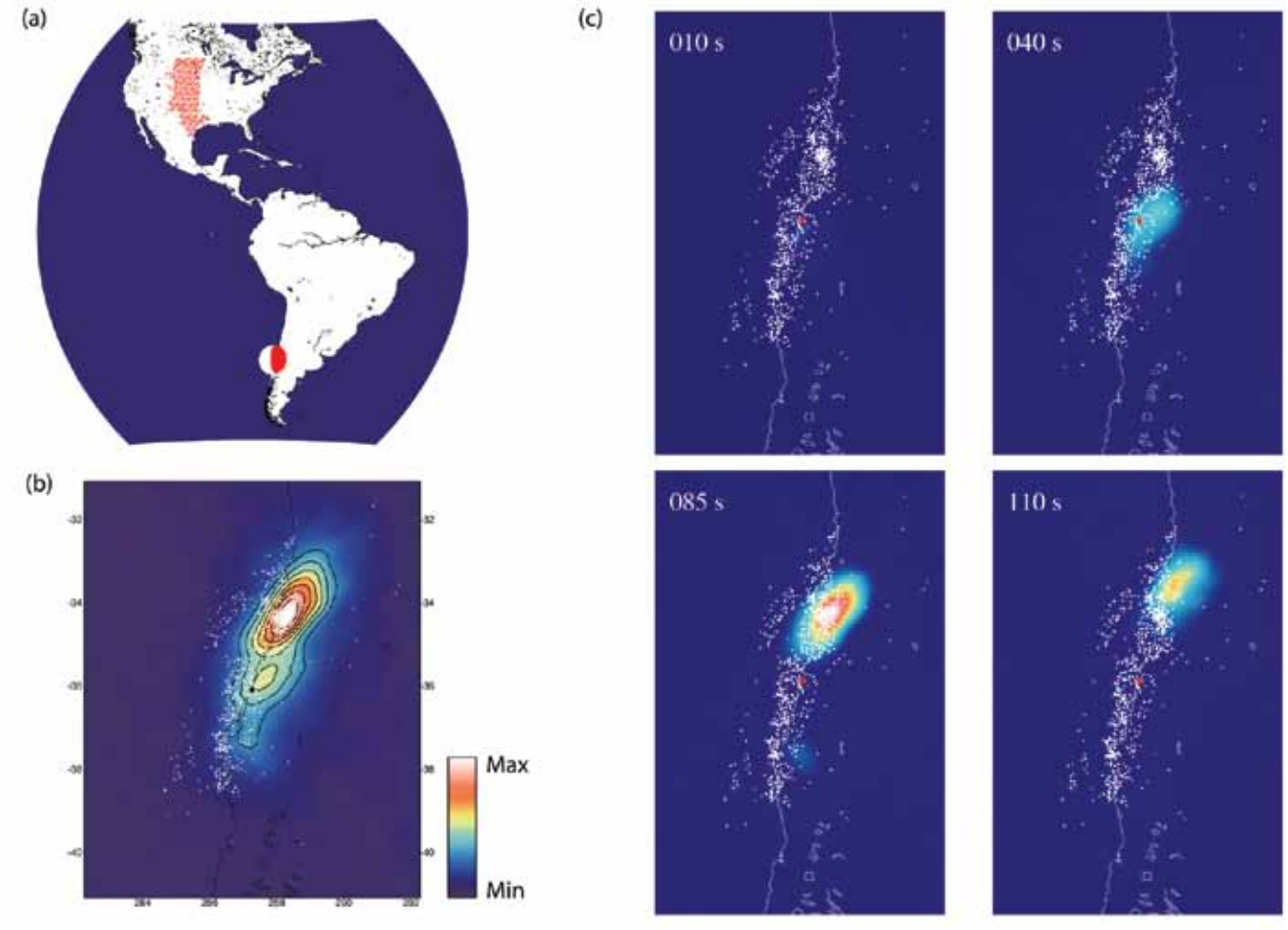

Back-projection results from the February 27, 2010, Mw8.8, Maule, Chile earthquake. (a) The distribution of TA stations (red triangles). (b) Relative energy release of the entire earthquake. The white dots are aftershocks. (c) Relative energy release at different times of the rupture.

Using MEMS Sensors and Distributed Sensing For a Rapid Array Mobilization Program (RAMP) Following the M8.8 Maule, Chile Earthquake

Jesse F. Lawrence *(Stanford University),* **Elizabeth S. Cochran** *(University of California, Riverside)*

The Quake-Catcher Network (QCN) exploits recent advances in sensing technologies and distributed sensing techniques. Micro-Electro-Mechanical Systems (MEMS) triaxial accelerometers are very low cost and interface to any desktop computer via USB cable enabling dense strong motion observations. Shake table tests show the MEMS accelerometers record high-fidelity seismic data and provide linear phase and amplitude response over a wide frequency range. Volunteer sensing using distributed computing techniques provides a mechanism to expand strong-motion seismology with minimal infrastructure costs, while promoting community participation in science. QCN has approximately 2000 participants worldwide that collect seismic data using a variety of MEMS sensors internal and external to computers. Distributed sensing allows for rapid transfer of metadata from participating stations, including data used to rapidly determine the magnitude and location of an earthquake. Trigger metadata are received with average data latencies between 3-7 seconds; the larger data latencies are correlated with greater server-station distances. Trigger times, wave amplitude, and station information are currently uploaded to the server for each trigger.

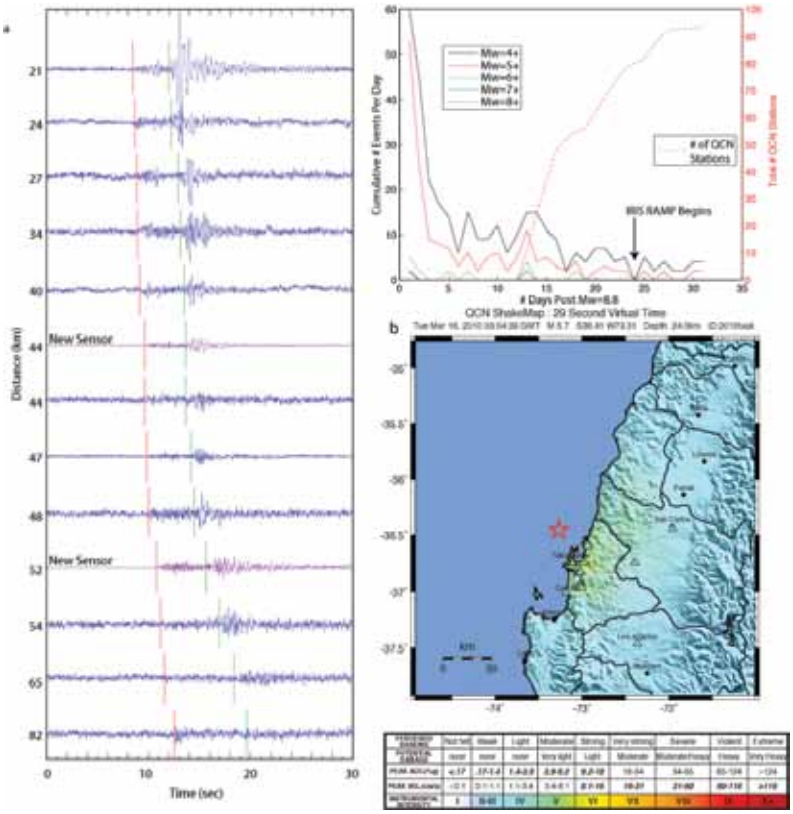

Figure 1: Left: Accelerograms from a M5.1 aftershock of the 27 February 2010 M8.8 Maule, Chile earthquake recorded on QCN stations in the Bio Bio region. Top right: Number of earthquakes and cumulative number of QCN stations installed versus days after the mainshock. Bottom right: Shake map produced using QCN records to locate and estimate the magnitude of the aftershock.

Following the 27 February 2010 M8.8 earthquake in Maule, Chile we initiated a QCN Rapid Aftershock Mobilization Program (RAMP) and installed 100 USB sensors to record aftershocks. The USB accelerators were deployed mainly in regions directly affected by the mainshock and were densely concentrated around ConcepciÃ³n. Using this data, we refined our triggering and event detection algorithms and tested, retrospectively, whether the network can rapidly and accurately identify the location and magnitude of the moderate to large aftershocks (M>4). Figure 1 illustrates QCNâ€™s ability to grow rapidly, record large aftershocks, and produce useful results such as earthquake locations and ShakeMaps. These results suggest that MEMS sensors installed in homes, schools, and offices provide a way to dramatically increase the density of strong motion observations for use in earthquake early warning. With QCNâ€™s low-latency real-time data collection strategy, future investigations with next-generation sensors will yield data pertinent to ground shaking, earthquake location, and rupture mechanics in near real-time.

References

Cochran, E.S., J.F. Lawrence, C. Christensen, and R. Jakka, The Quake-Catcher Network: Citizen science expanding seismic horizons, *Seismol. Res. Lett., 80*, 26-30,2009.

Cochran E., Lawrence J., Christensen C., Chung A., A novel strong-motion seismic network for community participation in earthquake monitoring, IEEE Inst & Meas, 12, 6, 8-15, 2009.

Acknowledgements: This work was preformed with support from NSF-EAR1035919, NSF-GEO0753435, and an IRIS subaward. We thank the thousands of volunteer participants who make the Quake-Catcher Network possible.

Teleseismic Inversion for Rupture Process of the 27 February 2010 Chile (Mw 8.8) Earthquake

Thorne Lay *(University of California Santa Cruz),* **Charles J. Ammon** *(The Pennsylvania State University),* **Hiroo Kanamori** *(California Institute of Technology),* **Keith D. Koper** *(Saint Louis University),* **Oner Sufri** *(Saint Louis University),* **Alexander R. Hutko** *(Incorporated Research Institutions for Seismology)*

The 27 February 2010 Chile (Mw 8.8) earthquake is the fifth largest earthquake to strike during the age of seismological instrumentation. The faulting geometry, slip distribution, seismic moment, and moment-rate function are estimated from broadband teleseismic P, SH, and Rayleigh wave signals obtained from Global Seismic Network and FDSN stations. We explore some of the trade-offs in the rupture-process estimation due to model parameterizations, limited teleseismic sampling of seismic phase velocities, and uncertainty in fault geometry. The average slip over the ~81,500 km2 rupture area is about 5 m, with slip concentrations down-dip, up-dip and southwest, and up-dip and north of the hypocenter. Relatively little slip occurred up-dip/offshore of the hypocenter. The average rupture velocity is ~2.0-2.5 km/s.

References

Lay, T., C. J. Ammon, H. Kanamori, K. D. Koper, O. Sufri, and A. R. Hutko (2010). Teleseismic inversion for rupture process of the 27 February 2010 Chile (Mw 8.8) earthquake, *Geophys. Res. Lett.*, in press.

Acknowledgements: This work was supported by NSF grant EAR0635570 and USGS Award Number 05HQGR0174.

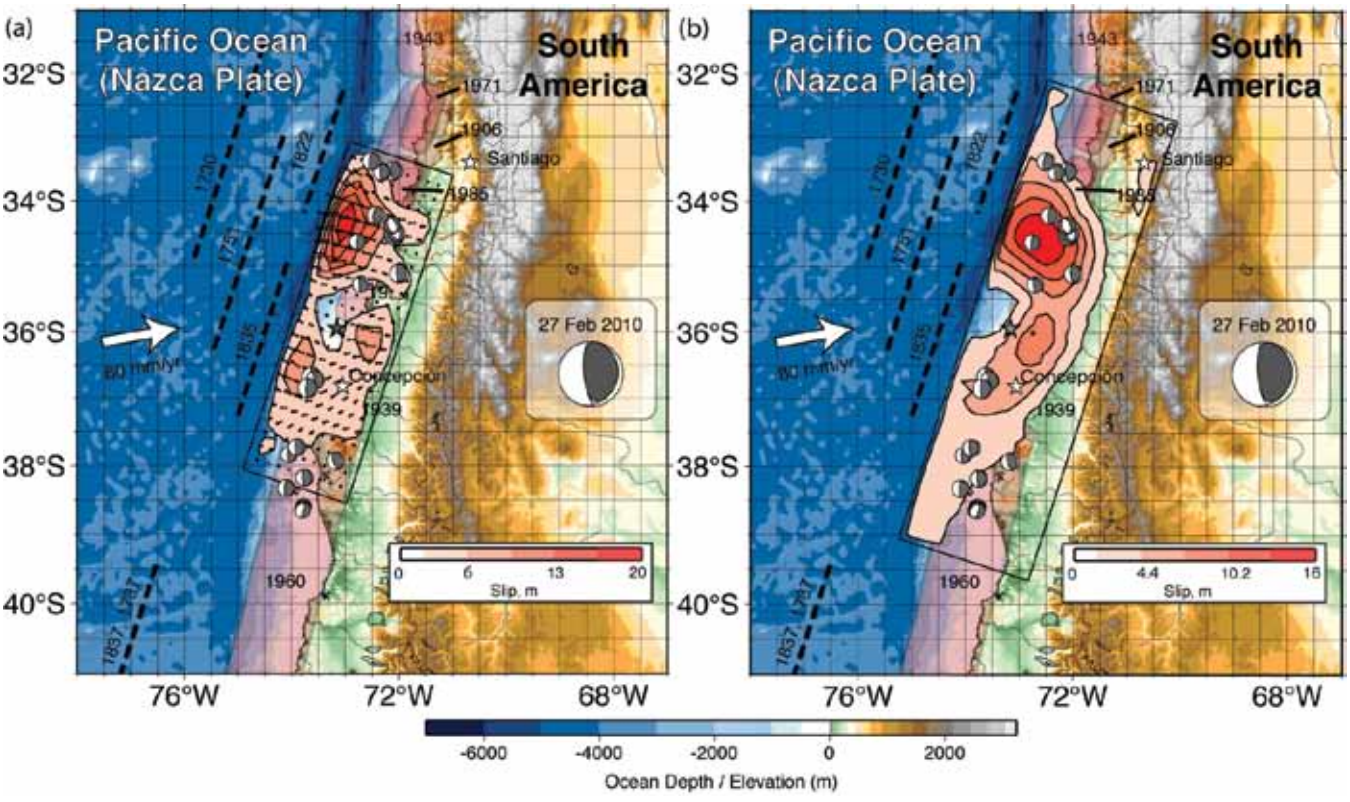

Maps of the finite-fault slip distributions obtained by inversion of (a) teleseismic P and SH waves and (b) teleseismic P waves, SH waves, and R1 STFs. The background map is the same as Figure 1, with the GCMT focal mechanism shown in the insets. The P and SH inversion allows for variable rake at each grid position, with the slip vectors for the hanging wall being shown, and their relative amplitudes contoured. The rupture velocity used for the P and SH inversion was 2.5 km/s and it was 2.25 km/s for the P, SH and R1 STF inversion.

The 2009 Samoa-Tonga Great Earthquake Triggered Doublet

Thorne Lay *(University of California Santa Cruz),* **Charles J. Ammon** *(The Pennsylvania State University),* **Hiroo Kanamori** *(California Institute of Technology),* **Luis Rivera** *(Institut de Physique du Globe de Strasbourg),* **Keith D. Koper** *(Saint Louis University),* **Alexander R. Hutko** *(U.S. Geological Survey, NEIC)*

Great earthquakes (having seismic magnitudes ≥ 8) usually involve abrupt sliding of rock masses at a boundary between tectonic plates. Such interplate ruptures produce dynamic and static stress changes that can activate nearby intraplate aftershocks, as is commonly observed in the trench-slope region seaward of a great subduction zone thrust event1-4. The earthquake sequence addressed here involves a rare instance in which a great trench-slope intraplate earthquake triggered extensive interplate faulting, reversing the typical pattern and broadly expanding the seismic and tsunami hazard. On 29 September 2009, within two minutes of the initiation of a moment magnitude 8.1 normal faulting event in the outer trench-slope at the northern end of the Tonga subduction zone, two major interplate underthrusting subevents (moment magnitudes = 7.8, 7.8), with total moment equal to a second great moment magnitude 8.0 earthquake, ruptured the nearby subduction zone megathrust. The collective faulting produced tsunami waves with localized regions of ~12 m run-up that claimed 192 lives in Samoa, American Samoa and Tonga. Overlap of the seismic signals obscured the fact that distinct faults separated by more than 50 km had ruptured with different geometries, with the triggered thrust faulting only being revealed by detailed seismic wave analyses. Extensive interplate and intraplate aftershock activity was activated over a large region of the northern Tonga subduction zone.

References

Lay, T., C. J. Ammon, H. Kanamori, L. Rivera, K. Koper, and A. R. Hutko (2010). The 29 September 2009 Great Samoa earthquake, *Nature*, in press.

Acknowledgements: This work was supported by NSF grant EAR0635570 and USGS Award Number 05HQGR0174.

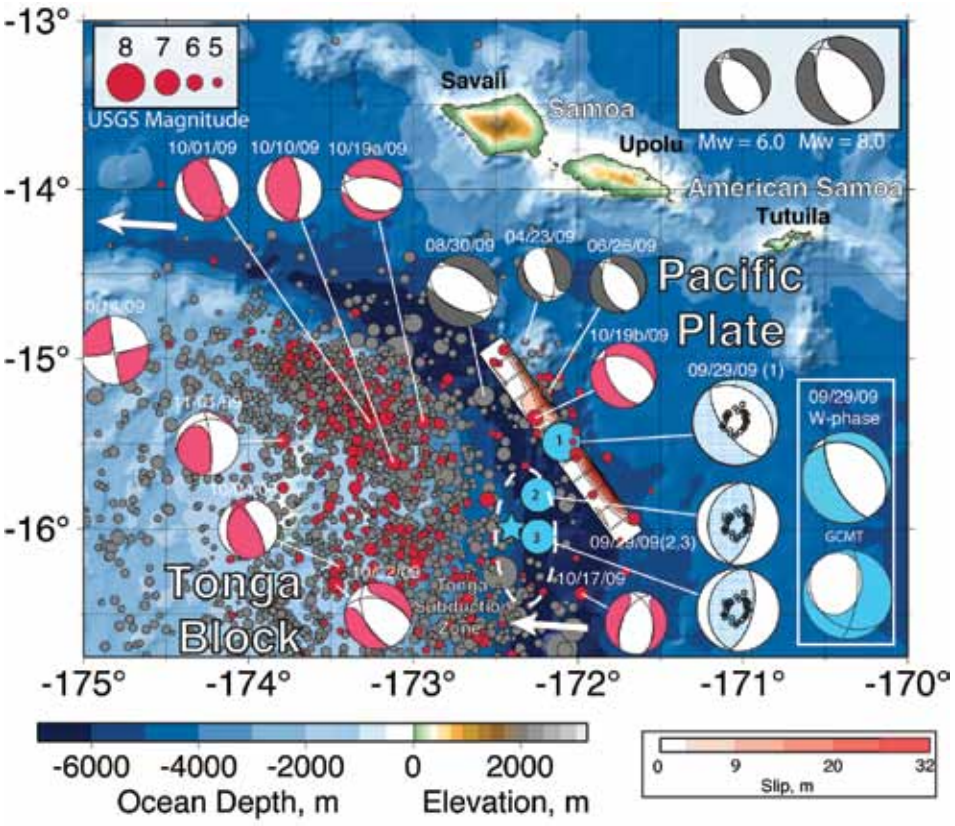

The great (Mw 8.1) 29 September 2009 Samoa earthquake ruptured an outer trench-slope normal fault (#1 blue mechanism and numbered blue circle) with the indicated fault plane and slip distribution and co-seismically triggered two initially unrecognized major (Mw 7.8, 7.8) thrust fault subevents (#2,3 blue mechanisms and circles) on the megathrust. The star indicates the centroid location estimated for event 3 from regional surface wave modeling. Gray circles indicate the locations and magnitudes of shallow (depth < 100 km) earthquakes from 01 January 1973 up to the 2009 great earthquake sequence, including three moderate-size (MW = 5 to 6.6) trench-wall/outer-rise extensional events between April and August 2009 for which global centroid-moment tensor17 solutions (gray coloring) are indicated (the Mw scaling of all GCMT solutions is indicated in the top right inset). Red circles indicate earthquake epicenters and magnitudes (top left inset gives the scaling) for the mainshock and aftershocks.

The Global Aftershocks of the 2004 Sumatra-Andaman Earthquake

Emily E. Brodsky *(UC Santa Cruz),* **Thorne Lay** *(UC Santa Cruz),* **Nicholas van der Elst** *(UC Santa Cruz)*

The 26 December 2004 Sumatra-Andaman Mw 9.15 earthquake was the largest earthquake to occur since the 1964 Alaska earthquake. In the subsequent 5.5 years, 9 great shallow earthquakes (M>= 8) have struck around the world giving a rate of 1.64 per year, whereas the prior century averaged 0.63 ± 0.34 per year.

Dynamic wave triggering effects combined with highly productive seismicity cascades could explain the rate increase. Seismic waves can trigger earthquakes to great distances. The resultant seismicity rate increase is observed to be proportional to the peak amplitude of the waves for a specific region (Fig. 1a). Over a broad swath of the globe, the 2004 Sumatra-Andaman earthquake generated ground velocities of over 0.01 cm/s (Fig. 1b), which are sufficient to trigger sizable rate changes (greater than a few percent) in susceptible regions (Fig 1a).

Once propagating seismic waves trigger a region, the remote sequences decay following Omori's Law [*Brodsky, 2006*]. Most of the triggered earthquakes are small, but each earthquake spawns further earthquakes, which occasionally can be larger than the initial events. These large events can in turn trigger other remote sequences.

References

Brodsky, E.E., *Geophys. Res. Lett., 33*, L15313, doi:10.1029/2006BL026605, (2006).

Jiang, C. and Z. Wu, H. Ma, L. Zhou, *Acta Seismologica Sinica, 3*, 189-200, (2009).

Van der Elst, N. J. and E. E. Brodsky, *J. Geophys. Res.*, doi:10.1029/2009JB006681, in press.

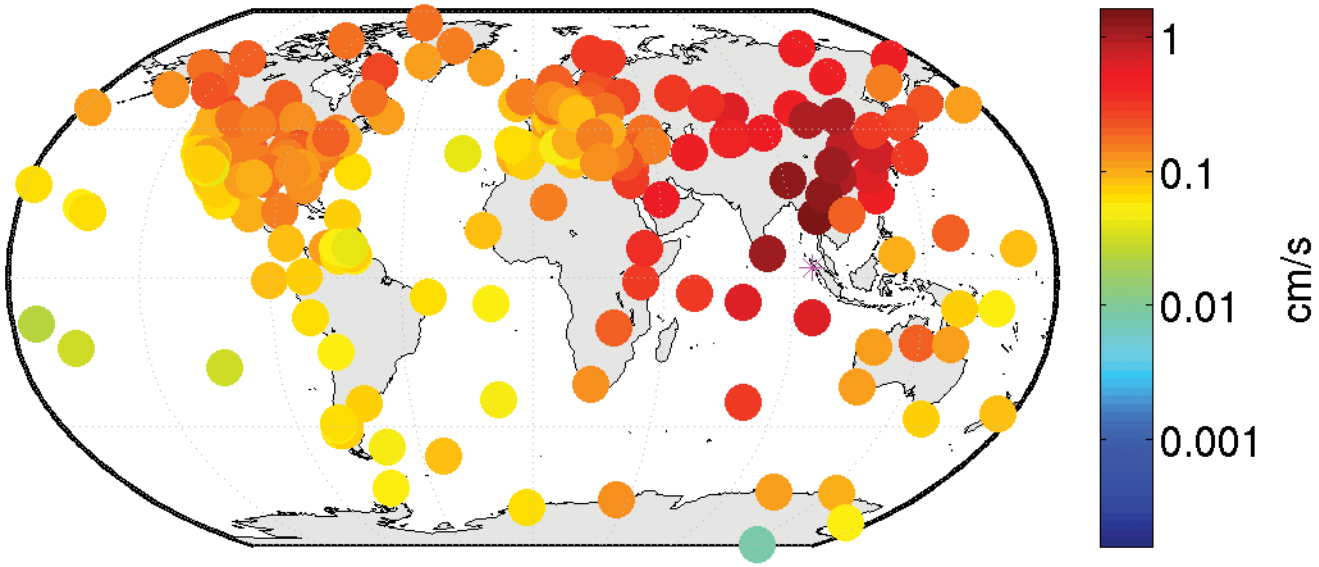

(a) Fractional earthquake rate increase as a function of peak dynamic strain from seismic waves [Van der Elst and Brodsky, in press]. The empirical relationship indicates that seismicity rates should increase significantly if ground shaking exceeds 0.01 cm/s. (b) Global map of recorded peak vertical ground velocities for the 2004 Sumatra-Andaman earthquake (epicenter at magenta star) indicating the widespread occurrence of strong shaking.

Temporal Changes of Surface Wave Velocity Associated with Major Sumatra Earthquakes from Ambient Noise Correlation

Zhen J. Xu *(Department of Geology, University of Illinois at Urbana-Champaign),* **Xiaodong Song** *(Department of Geology, University of Illinois at Urbana-Champaign)*

Detecting temporal changes of medium associated with major earthquakes has major implications for understanding earthquake genesis. The recent development of passive imaging through cross correlation of diffusive wavefield provides great opportunity in monitoring such changes because of the complete repeatability of the data processing procedures. We acquired 54 months of long period continuous data from Jan. 2004 to Jun. 2008 for stations in the Southeast Asia region from IRIS DMC. The stations are operated by GSN, Malaysia, Japan, and China. We retrieved empirical Green's functions (EGFs) of surface wave between stations through cross correlation of continuous ambient noise data [*Bensen et al., 2007*]. We compared EGFs at different time periods before and after earthquake with a reference EGF. We observed clear temporal changes up to 1.44 s in Rayleigh wave after three major earthquakes in Sumatra region in Dec. 2004, Mar. 2005, and Sep. 2007 and a plausible precursor signal before Dec. 2004 event. However such changes were absent in Love waves. The temporal changes in Rayleigh wave appeared over a broad area near the source for a few months after the earthquakes and are frequency dependent. The observations are interpreted as stress changes and subsequent relaxation in upper-mid crust in the immediate vicinity of the rupture and the broad area near the fault zone.

References

Bensen, G. D., et al. (2007) Processing seismic ambient noise data to obtain reliable broad-band surface wave dispersion measurements. *Geophys. J. Int. 169*: 1239-1260

Acknowledgements: All data were downloaded from IRIS DMC. This work was supported by NSF (EAR8038188) and AFRL (FA8718-07-C-0006)

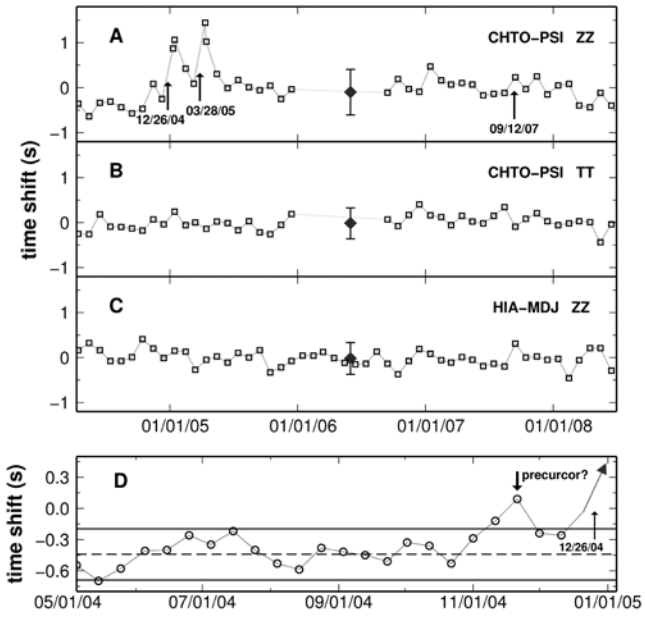

Time shifts of various station pairs, relative to reference stack of all time periods. (A-C) Rayleigh wave for CHTO-PSI from vertical (Z) component correlation (A), Love wave for CHTO-PSI from tangential (T) component correlation (B), and a stable reference pair HIA-MDJ outside Sumatra region in northeast China (C). (D) Enlarged view of time shifts of CHTO-PSI Rayleigh wave before Dec. 2004 event.

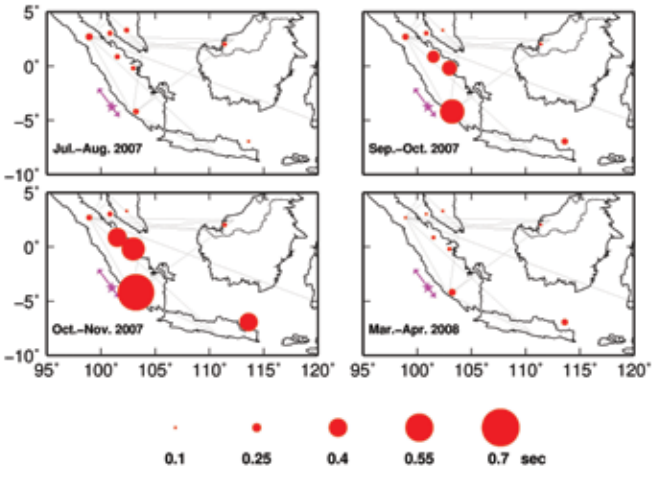

Snapshots of time-shift maps before (upper left), during (Upper Right), and after (Lower, left and Right) the 2007 event.

The 17 July 2006 Java Tsunami Earthquake (Mw = 7.8)

Charles J. Ammon *(Department of Geosciences, The Pennsylvania State University),* **Hiroo Kanamori** *(Seismological Laboratory, California Institute of Technology),* **Thorne Lay** *(Department of Earth and Planetary Sciences, Univ. California Santa Cruz),* **Aaron A. Velasco** *(Department of Geological Sciences, Univ. Texas El Paso)*

The 17 July 2006 Java earthquake involved thrust faulting in the Java trench and excited a deadly tsunami (~ 5-8 m) that inundated the southern coast of Java. The earthquake's size estimates vary significantly with seismic wave period: very long-period signals (300-500+ s) indicate a seismic moment of 6.7 x 10**20 Nm (Mw = 7.8), Ms (~20 s) = 7.2, mb (~1 s) = 6.2, while shaking intensities (3-10 Hz) were ≤ MMIV. The large tsunami relative to Ms characterizes this event as a tsunami earthquake. Like previous tsunami earthquakes, the Java event had an unusually low rupture speed of 1.0-1.5 km/s, and occurred near the up-dip edge of the subduction zone thrust fault. Most large aftershocks involved normal faulting. The rupture propagated ~200 km along the trench, with several pulses of shorter period seismic radiation superimposed on a smooth background rupture with an overall duration of ~185 s. The rupture process was analyzed using finite fault inversion of P, SH, and Rayleigh wave source time functions, with the excellent quality of the data providing good resolution of the rupture velocity (Ammon et al., 2006). This is the best recorded tsunami earthquake since the 1992 Nicaragua rupture, and the great expansion of broadband data since that time enables much more robust characterization of the anomalous source process.

References

Ammon, C. J., H. Kanamori, T. Lay, and A. A. Velasco (2006), The 17 July 2006 Java tsunami earthquake, *Geophys. Res. Lett.*, 233, L234308, doi:10.10239/2006GL028005.

Acknowledgements: The facilities of the IRIS Data Management System were used to access the data used in this study.

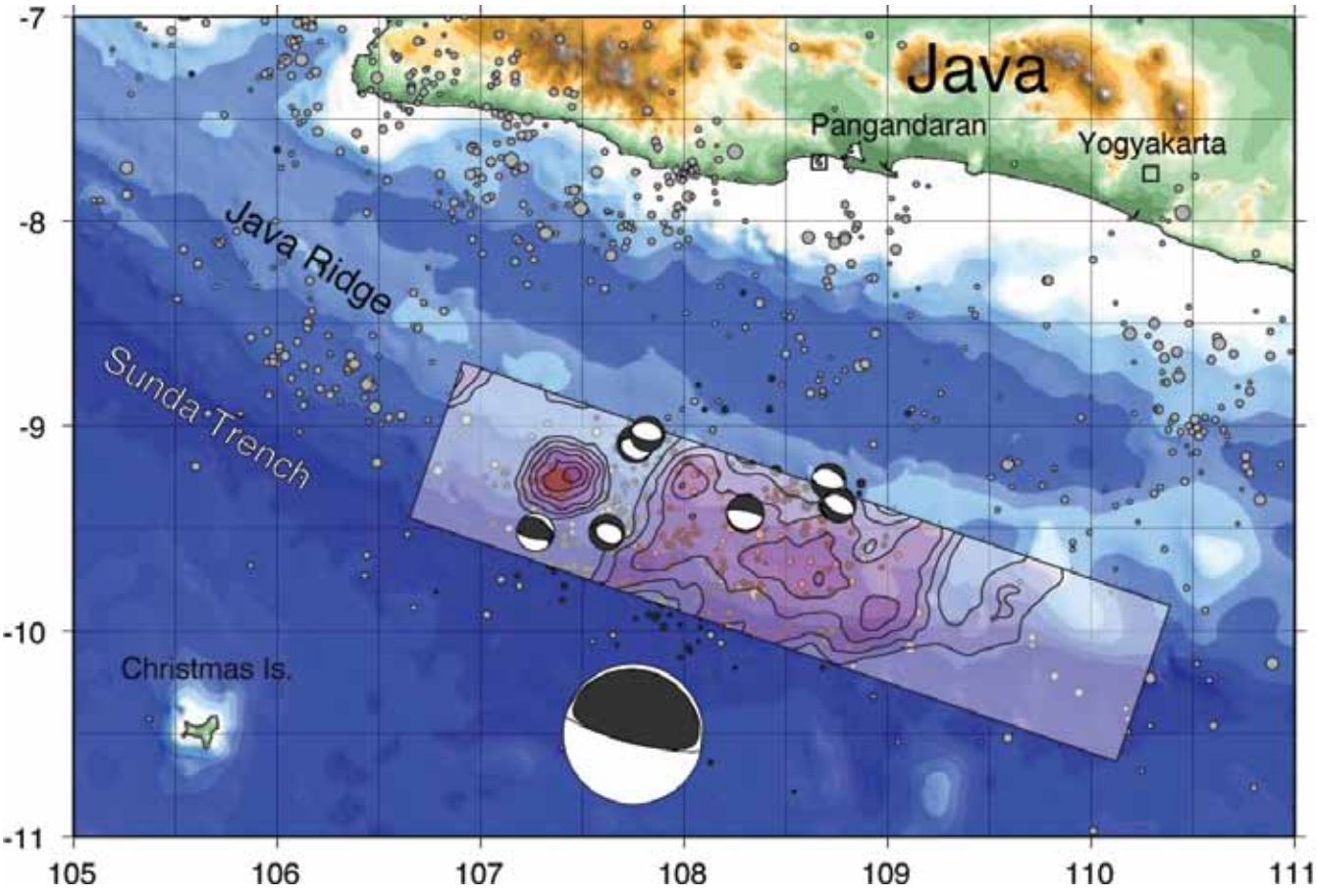

Map showing the Global CMT solutions for the 17 July 2006 Java tsunami earthquake and regional aftershocks and NEIC epicenters of mainshock (star), aftershocks (dark circles), and prior activity (gray circles).

Tsunami Early Warning Using Earthquake Rupture Duration and P-Wave Dominant-Period: The Importance of Length and Depth of Faulting

Anthony Lomax *(ALomax Scientific, Mouans-Sartoux, France),* **Alberto Michelini** *(Istituto Nazionale di Geofisica e Vulcanologia, Rome)*

After an earthquake, rapid, real-time assessment of hazards such as ground shaking and tsunami potential is important for early warning and emergency response. Tsunami potential depends on sea floor displacement, which is related to the length, L, width, W, mean slip, D, and depth, z, of earthquake rupture. Currently, the primary discriminant for tsunami potential is the centroid-moment tensor magnitude, MwCMT, representing the product LWD, and estimated through an indirect, inversion procedure. The obtained MwCMT and the implied LWD value vary with the depth of faulting, assumed earth model and other factors, and is only available 30 min or more after an earthquake. The use of more direct procedures for hazard assessment, when available, could avoid these problems and aid in effective early warning. Here we present a direct procedure for rapid assessment of earthquake tsunami potential using two, simple measures on P-wave seismograms – the dominant period on the velocity records, Td, and the likelihood that the high-frequency, apparent rupture-duration, T0, exceeds 50-55 sec. Td and T0 can be related to the critical parameters L, W, D and z. For a set of recent, large earthquakes, we show that the period-duration product TdT0 gives more information on tsunami impact, It, and size, At, than MwCMT and other currently used discriminants. All discriminants have difficulty in assessing the tsunami potential for oceanic strike-slip and back-arc, intraplate earthquake types. Our analysis and results suggest that tsunami potential is not directly related to the product LWD from the "seismic" faulting model, as is assumed with the use of the MwCMT discriminant. Instead, knowledge of rupture length, L, and depth, z, alone can constrain well the tsunami potential of an earthquake, with explicit determination of fault width, W, and slip, D, being of secondary importance. With available real-time seismogram data, rapid calculation of the direct, period-duration discriminant can be completed within 6-10 min after an earthquake occurs and thus can aid in effective and reliable tsunami early warning.

References

Lomax, A., and A. Michelini (2009), Tsunami early warning using earthquake rupture duration, *Geophys. Res. Lett., 36,* L09306.

This work Submitted to *Geophys. J. Int.,* 2 Apr 2010.

Acknowledgements: This work is supported by the 2007-2009 Dipartimento della Protezione Civile S3 project. The IRIS DMC (http://www.iris.edu) provided access to waveforms used in this study; we thank all those who install, operate and maintain seismic stations worldwide.

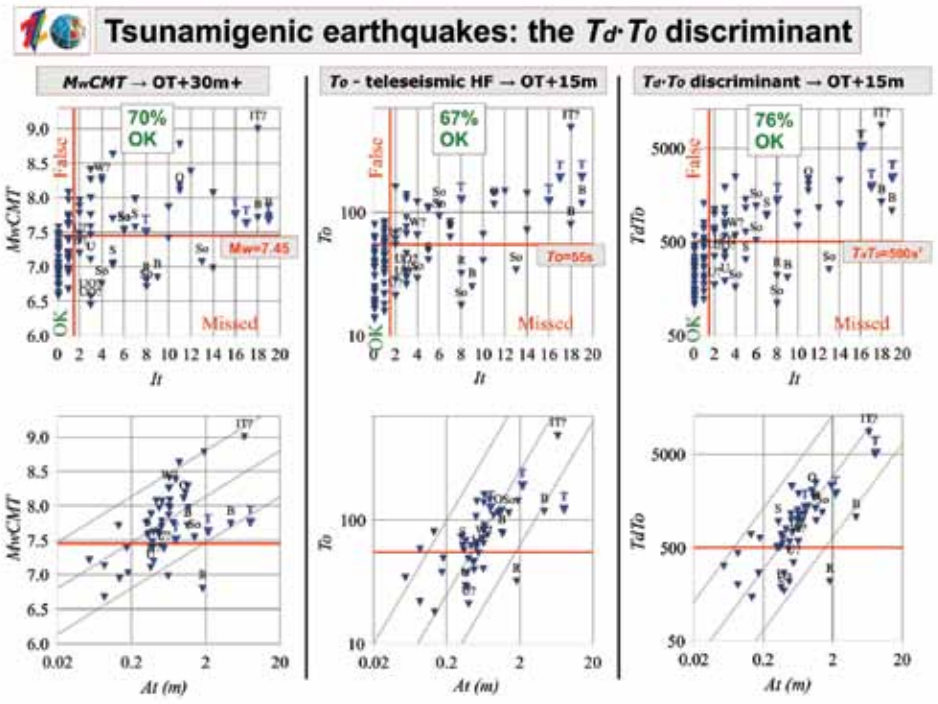

Comparison of centroid-moment tensor magnitude, M_w^{CMT}, (left column), apparent source duration, T_0, (centre column) and teleseismic, period-duration, T_dT_0, (right column) with tsunami importance, I_t, (upper row) and representative tsunami amplitude at 100km, A_t, (lower row). Vertical red lines show the target $I_t \geq 2$ threshold; horizontal red lines show the optimal cutoff values for the M_{wp}, M_w^{CMT}, T_0 and T_dT_0 discriminants; quadrants containing correctly identified tsunamigenic and non-tsunamigenic events are labelled "OK"; quadrants containing incorrectly identified events are labelled "Missed" and "False". The A_t and T_0 axes use logarithmic scaling. Diagonal lines show possible linear relationships between A_t and M_0 (lower left), T_0 (lower centre) and T_dT_0 (lower right). Event labels show earthquakes type for non interplate-thrust events with $I_t \geq 2$ (I–interplate-thrust; T–tsunami earthquake (blue); O–outer-rise intraplate; B–back-arc or upper-plate intraplate; So–strike-slip oceanic, S–strike-slip continental, R–reverse-faulting).

Seismic Cycles on Oceanic Transform Faults

Jeff McGuire *(WHOI),* **Margaret Boettcher** *(University of New Hampshire),* **John Collins** *(WHOI)*

The long-standing hypothesis that the timing of the largest earthquakes is primarily controlled by quasi-periodic seismic cycles, where stress builds up for an extended period of time and then is released suddenly in a large earthquake, has been difficult to verify due to the long repeat times (50-1000 years) of the largest earthquakes on most faults. By contrast, repeat times of the largest oceanic transform fault earthquakes are remarkably short and regular. Thermal processes appear to have a strong control on oceanic transform seismicity including the magnitude of the largest earthquake on a particular fault [Boettcher and Jordan, 2004]. Using datasets from the Global Seismic Network that span 20+ years of recording at the same sites, we determined that the largest earthquakes on warm EPR transform faults repeat every ~5 years on a relatively regular cycle [McGuire, 2008]. Moreover, the duration of the seismic cycle increases for colder faults according to a simple scaling relation [Boettcher and McGuire, 2009]. The quasi-periodic nature of oceanic transforms seismic cycles allowed us to successfully position an array of ocean bottom seismometers on the Gofar Transform Fault to capture a Mw 6.0 earthquake in 2008. Our successful experiment on the Gofar Fault has further demonstrated that oceanic transform faults have predictable seismic characteristics including relatively regular seismic cycles.

References

Boettcher, M. S., and T. H. Jordan (2004), Earthquake Scaling Relations for Mid-Ocean Ridge Transform Faults, *J. Geophys. Res.*, B12302, doi:1029/2004JB003110.

Boettcher, M. S., and J. J. McGuire (2009), Scaling relations for seismic cycles on mid-ocean ridge transform faults, *Geophys. Res. Lett., 36*, L21301, doi:21310.21029/22009GL040115.

McGuire, J. J. (2008), Seismic Cycles and Earthquake Predictability on East Pacific Rise Transform Faults, *Bull. Seismol. Soc. Amer., 98*, 1067-1084, doi: 1010.1785/0120070154.

Acknowledgements: We thank the Global Seismic Network program for collecting the datasets over the last 20+ years that were necessary for us to conduct this research.

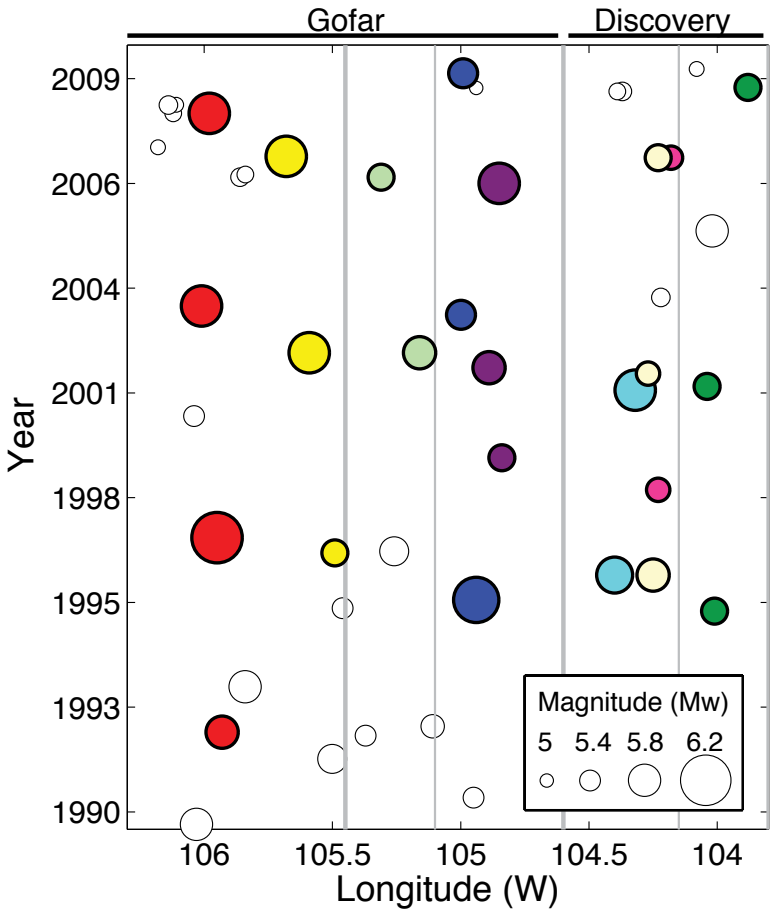

Figure 1. Updated after McGuire [2008]. Earthquakes in the Global CMT catalogs for the Gofar and Discovery transform faults for the time period from 1990–2010. Pairs of MW ≥ 5.5 mainshocks that have been determined to have overlapping rupture areas are shown with matching colors and are not at exactly the same longitude due to errors in the CMT location estimates. Major and minor spreading centers are shown by thick and thin gray lines, respectively.

Split Normal Modes and Beachfront Hotels

Seth Stein *(Northwestern University)*

On December 26, 2004 a giant earthquake beneath the Indonesian island of Sumatra generated a massive tsunami that crossed the Indian Ocean in a few hours, wreaking destruction along seacoasts and causing at least 250,000 deaths. Initial seismological studies suggested that only part of the 1200-km long fault zone had broken, so an even larger earthquake could be forthcoming. However, analysis of the splitting pattern of earth's longest period (> 20 minute) normal modes using IRIS broadband data showed that the entire fault zone had ruptured. This result explained the perplexing pattern of the tsunami damage. Combining these data with the motions of the plates involved measured by combining seafloor magnetic data and high-precision GPS then implied that such earthquakes should occur about 500 years apart, as later confirmed by paleotsunami studies. Hence contrary to initial fears, rebuilding the crucial tourist facilities at their previous locations made sense.

The December earthquake also give insight into the long-standing question of which trenches can have such giant earthquakes. The earthquake was much larger than expected from a previously proposed relation, based on the idea of seismic coupling, in which such earthquakes occur only when young lithosphere subducts rapidly. Moreover, a global reanalysis finds little support for this correlation. Hence it appears that much of the apparent differences between subduction zones, such as some trench segments but not others being prone Mw> 8.5 events and hence oceanwide tsunamis, may reflect the short earthquake history sampled. This possibility is supported by the variability in rupture mode at individual trench segments.

References

Stein, S., and E. A. Okal, Speed and size of the Sumatra earthquake, *Nature, 434*, 581-582, 2005.

Stein, S. and E. Okal, Ultralong period seismic study of the December 2004 Indian Ocean earthquake and implications for regional tectonics and the subduction process, B*ull. Seismol. Soc. Amer., 97*, S279-S295, 2007.

Stein, S. and E. Okal, Observations of ultralong period normal modes from the December 2004 Sumatra-Andaman earthquake, *Phys. Earth Planet. Int., 175* 53-62, 2009.

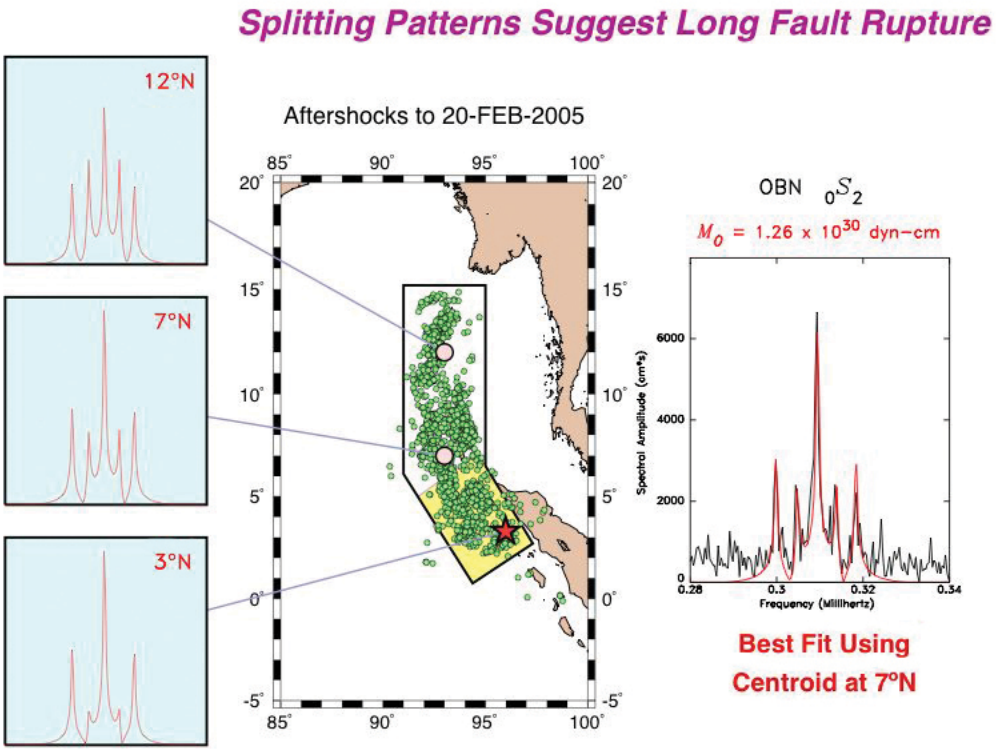

Split singlet pattern for 0S2 normal mode multiplet showing dependence on source latitude. Map at center illustrates the two possible models of source rupture: the short fault initially inferred from body wave inversion and the long fault suggested by the distributions of aftershocks (small circles). The diagrams at left show theoretical splitting patterns at Obninsk, Russia (OBN) for sources located at the original USGS epicenter (3°N; star), at 7°N, and towards the northern end of the long fault (12°N). The right panel shows that the best fit occurs for a centroid of moment release at 7°N, at the center of the aftershock zone but outside the rupture zone of the short fault model. (Stein and Okal, 2007)

Migration of Early Aftershocks Following the Mw6.0 2004 Parkfield Earthquake

Zhigang Peng *(Georgia Institute of Technology),* **Peng Zhao** *(Georgia Institute of Technology)*

A large shallow earthquake is immediately followed by numerous aftershocks with a significant portion missing in existing earthquake catalogs, mainly due to masking of the mainshock coda and overlapping arrivals [e.g., Peng et al., 2006]. Recovering these missing early aftershocks is important for understanding the physical mechanisms of earthquake triggering, and tracking post-seismic deformation around the mainshock rupture zone. We use waveforms of relocated events along the Parkfield section of the San Andreas Fault (SAF) as templates, and scan through continuous waveforms for 3 days around the 2004 Mw6.0 Parkfield earthquake to detect missing aftershocks [Peng and Zhao, 2009]. We identify 11 times more aftershocks than reported in the standard Northern California Seismic Network (NCSN) catalog. The newly detected aftershocks show clear migration in both along-strike and down-dip directions with logarithmic time since the mainshock, consistent with the numerical simulations on expansions of aftershocks caused by propagating afterslip. The cumulative number of early aftershocks increases linearly with postseismic deformation in the first 2 days, supporting the view that aftershocks are driven primarily by afterslip.

References

Peng, Z., J. E. Vidale, and H. Houston (2006), Anomalous early aftershock decay rates of the 2004 M6 Parkfield earthquake, *Geophys. Res. Lett.*, *33*, L17307, doi:10.1029/2006GL026744.

Peng, Z., and P. Zhao (2009), Migration of early aftershocks following the 2004 Parkfield earthquake, *Nature Geosci.*, 2, 877-881, doi:10.1038/ngeo697.

Acknowledgements: This work was supported by the USGS NEHRP program G09AP00114.

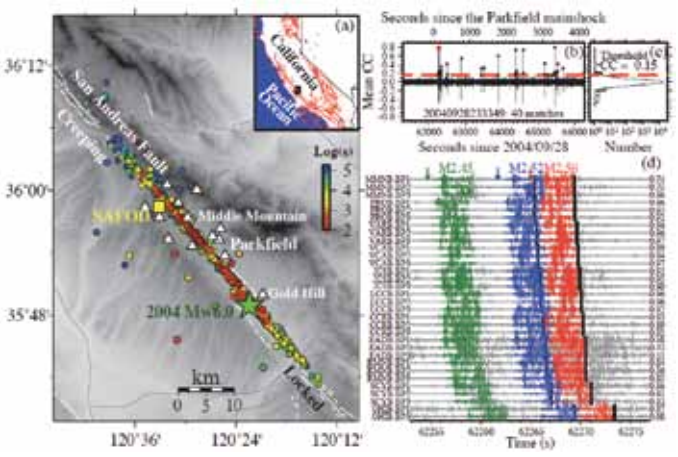

Newly detected aftershocks showing migrations after the 2004 Mw6.0 Parkfield earthquake. (a) Map of the Parkfield section of the San Andreas Fault (SAF; white lines). The newly detected aftershocks are color-coded by their occurrence times (in logarithmic scales) since the Parkfield mainshock (green star). (b) Mean cross-correlation (CC) functions for the template event 20040928233349. The black dots are positive detections above the threshold (red dashed line) and the red dot corresponds to the detected M2.56 event at ~140 s after the mainshock. (c) The histogram of the mean CC functions. (d) A comparison of the template waveforms (red) and the continuous waveforms (gray) for each component of 11 stations. Waveforms shown in green and blue colors correspond to other two events that occurred nearby. The arrows mark the origin times of the three events.

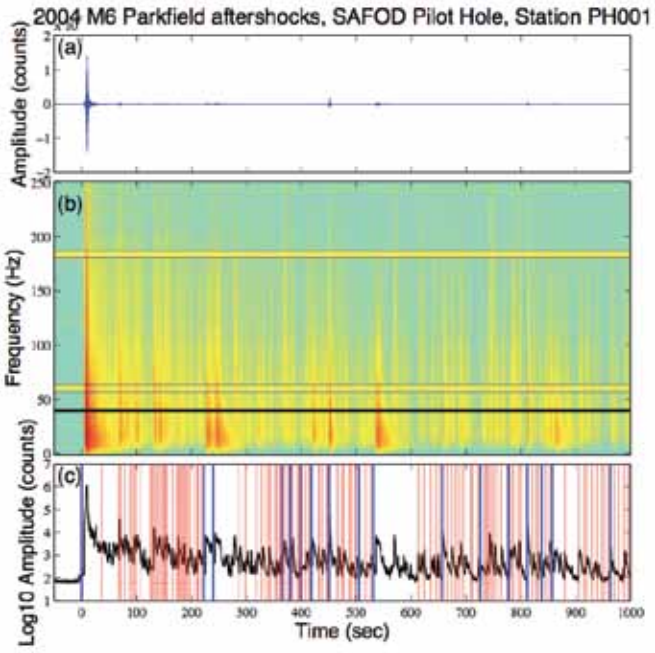

Early aftershocks of the 2004 Parkfield earthquake recorded by the SAFOD Pilot Hole station. (a) The raw vertical-component seismogram recorded at the SAFOD Pilot Hole station PH001 within the first 1000 s after the 2004 Mw6.0 Parkfield earthquake. (b) The corresponding spectrogram of (a) showing the mainshock and numerous early aftershocks. The think horizontal line at 40 Hz marks the corner of the high-pass filter, and the thin bands around 60 and 184 Hz mark the continuous electronic noise. (c) The envelope functions of the median-averaged spectrogram above 40 Hz. The vertical blue and red lines mark the origin times of 16 and 130 aftershocks listed in the NCSN catalog and detected by our technique, respectively.

Mapping Subduction Zone Fault Slip with Teleseismic and Geodetic Data

Matthew E. Pritchard *(Cornell University),* **Chen Ji** *(University of California, Santa Barbara),* **Eric Fielding** *(Jet Propulsion Lab),* **Jack Loveless** (*Harvard University),* **Mark Simons** *(Caltech), Tim Dixon (University of Miami)*

In an effort to understand the behavior of the megathrust fault in the Peru-Chile subduction zone, we have used seismic and geodetic observations to determine the location of fault slip during different parts of the earthquake cycle (co-seismic, post-seismic, and inter-seismic). During the co-seismic time period, we can invert teleseismic waveforms from the GSN and geodetic data (InSAR and GPS) both jointly and separately to constrain the rupture process. We have combined the seismic and geodetic data to study 8 earthquakes (6.7 < Mw < 8.4) in southern Peru and northern Chile that occurred between 1993 and 2007 (Fig. 1), providing one of the most detailed space-time rupture histories available in a subduction zone and yielding new discoveries about the generation of large earthquakes in this area [Pritchard et al., 2006; Pritchard et al., 2007; Pritchard & Fielding, 2008; Loveless et al., 2010]. In northern Chile, because of the spatially and temporally dense geodetic data and constraints on earthquake locations and slip from the GSN, we can clearly separate co-seismic and post-seismic deformation. We document a complex mosaic of phenomena including large earthquakes, post-seismic after-slip with a spatial distribution that appears to be tied to variations in coastal morphology, and the first observations with sufficient resolution in both time and space to infer triggering of a large (Mw > 7) earthquake by a so-called ``silent earthquake" [Pritchard & Simons, 2006]. Using the teleseismic and geodetic data together, we have shown that in order to make reliable two-dimensional models of earthquake slip for subduction zone earthquakes larger than magnitude 7.5 (necessary for hazard and other types of studies), we cannot use standard techniques. We must either combine teleseismic data with the geodetic data [Pritchard et al., 2007; Pritchard & Fielding, 2008] or use new analysis methods recently developed by others [Lay et al., 2010]. We used our detailed models of the 6 largest earthquakes to study potential relationships between the rupture areas and other observables in an effort to better forecast the location of large earthquakes. We find no obvious or simple relationship between various other proposed physical processes and the earthquake slip in these earthquakes. However, analysis of the forearc gravity field and its gradients shows correlation with many of the observed slip patterns, as suggested by previous studies [Loveless et al., 2010].

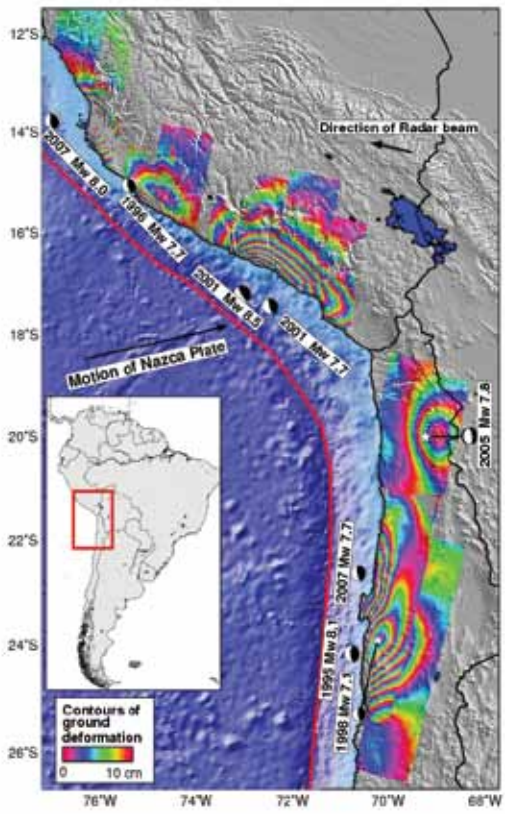

Contours of ground deformation (10 cm interval) from some large subduction zone earthquakes in the central Andes as measured by the ERS-1, ERS-2 and Envisat satellites of the European Space Agency. Deformation is in the line-of-sight of the radar beam, which is about 23 degrees from vertical and projected onto the map as a black arrow. The largest magnitude of ground deformation during the earthquakes is off-shore, but these dense on-land images of ground displacement provide new information about the details of the fault motion during the earthquake.

References

J. P. Loveless, M. E. Pritchard, and N. Kukowski, Testing mechanisms of subduction zone segmentation and seismogenesis with slip distributions from recent Andean earthquakes, *Tectonophysics, 2009*, in press.

M. E. Pritchard, and E. J. Fielding, A study of the 2006 and 2007 earthquake sequence of Pisco, Peru, with InSAR and teleseismic data, *Geophys. Res. Lett., 35*, 10.1029/2008GL033374, 2008.

M. E. Pritchard, E. Norabuena, C. Ji, R. Boroschek, D. Comte, M. Simons, T. Dixon, and P. A. Rosen, Teleseismic, geodetic, and strong motion constraints on slip from recent southern Peru subduction zone earthquakes, *J. Geophys. Res., 112*, 10.1029/2006JB004294, 2007.

M. E. Pritchard, and M. Simons, An aseismic fault slip pulse in northern Chile and along-strike variations in seismogenic behavior, *J. Geophys. Res., 111*, 10.1029/2006JB004258, 2006.

M. E. Pritchard, C. Ji, and M. Simons, Distribution of slip from 11 Mw > 6 earthquakes in the northern Chile subduction zone, *J. Geophys. Res., 111,* 10.1029/2005JB004013, 2006.

Apparent Stress Variations at the Osa Peninsula, Costa Rica, Influenced by Subducted Bathymetric Features

Pamela A. Moyer *(Earth and Environ. Science Dept., New Mexico Tech),* **Susan L. Bilek** *(Earth and Environ. Science Dept., New Mexico Tech),* **W. Scott Phillips** *(Earth and Environ. Sciences Div., Los Alamos Natl. Lab.)*

Subducted bathymetric features such as seamounts have been modeled as areas of strong frictional behavior between the subducting and overriding plates. These models describe subducted features as "sticking" to the overriding plate, thereby increasing stress at the feature until slip occurs. On the Pacific Coast of Costa Rica, a number of bathymetric features enter the Middle America Trench near the Osa Peninsula (Figure 1). Using data collected and processed through a PASSCAL experiment from six land seismometers and data from twelve ocean bottom seismometers, aftershocks of the 1999 6.9 Mw Quepos thrust-faulting event were analyzed to investigate the influence subducted features have on earthquake rupture near the Osa Peninsula. Apparent stress values between 0.1 MPa and 2.5 MPa were found for 114 aftershocks using seismic coda techniques. An average apparent stress value two times higher than the global average apparent stress value for thrust-faulting events at oceanic subduction zones was found for the analyzed events. The range of apparent stress values observed near the Osa Peninsula, and high average value, suggests areas of stress concentration along the subduction interface as a result of strong frictional behavior due to bathymetric features at depth.

References

Moyer, P.A., S.L. Bilek, and W.S. Phillips (2009), Apparent stress variations at the Osa Peninsula, Costa Rica, and the role of subducting topography, EOS Trans AGU, 90(52), Fall Meet. Suppl., Abstract T23B-1892.

Acknowledgements: We gratefully acknowledge NSF funding for this project NSF-OCE 0751610 to SLB.

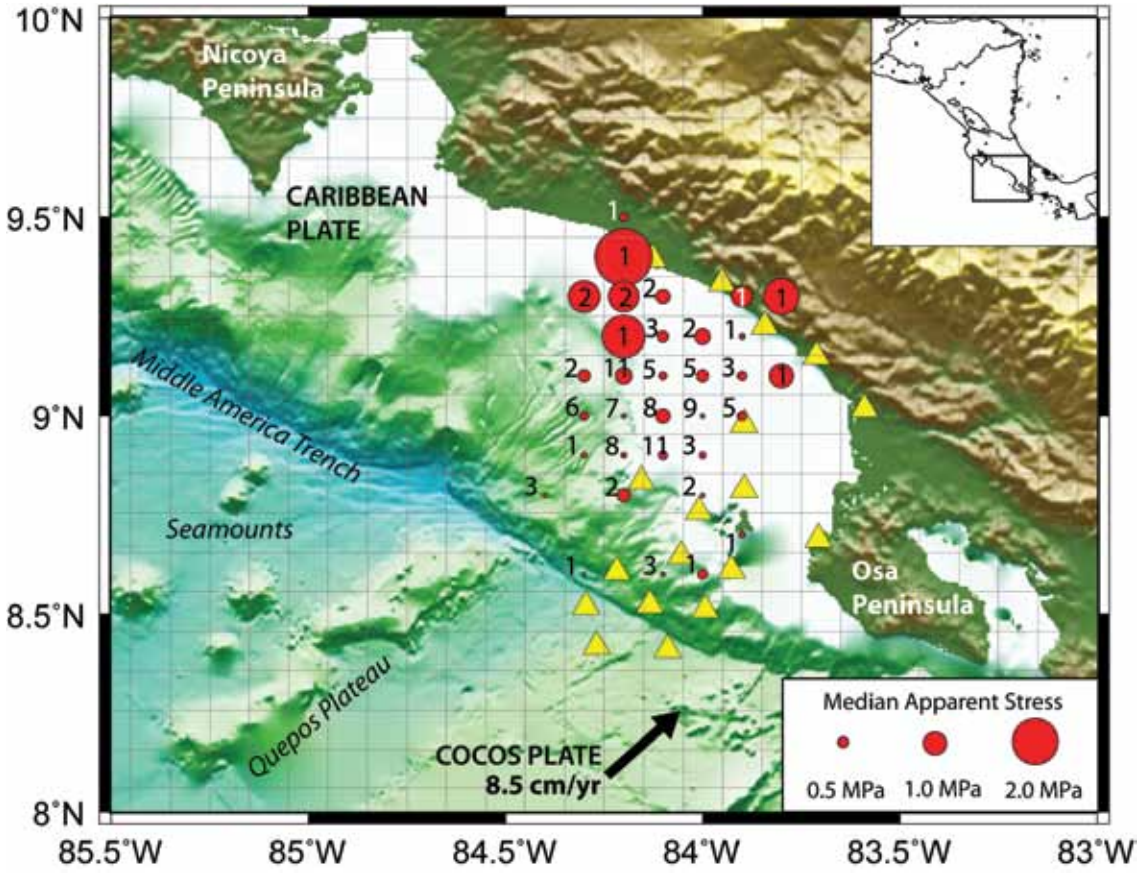

Median apparent stress values for events near the Osa Peninsula, Costa Rica in 0.1 x 0.1 degree grids. The size of the red circle indicates the median value of apparent stress for events within that grid. Numbers of events used to compute the median within each grid are noted. Yellow triangles are land and ocean bottom seismometers used in this study. A range of apparent stress values was observed near the Osa Peninsula with concentrations of high apparent stress indicative of strong frictional behavior along the subduction interface due to bathymetric features at depth.

Deep Earthquake Mechanics, Slab Deformation, and Subduction Forces

Linda M. Warren (*Saint Louis University*)

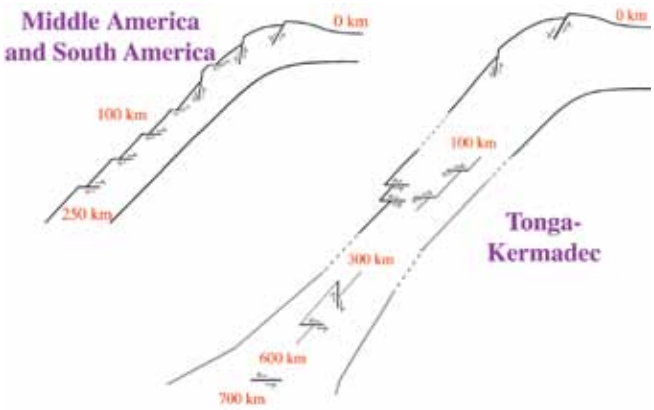

Schematic cross-section showing fault orientations in subducting slabs.

Deeper than ~50 km depth in the Earth, the confining pressure is so high that it should prevent earthquakes from occurring. However, subduction zone earthquakes occur down to ~700 km depth. Based of the stability of minerals in the subducting lithosphere, mechanisms such as dehydration embrittlement and transformational faulting have been proposed for generating the earthquakes. These mechanisms have different implications for the orientation of earthquake fault planes, so they can be tested by identifying fault planes. Applying a method developed by Warren and Silver [*2006*] to data from all available seismic networks, we analyze the directivity of 200 large deep earthquakes in the Tonga [*Warren et al, 2007a*], Middle America [*Warren et al, 2008*], and central South America [*Warren et al, 2007b*] subduction zones to identify the fault planes for ~1/4 of the earthquakes. Despite large differences in temperature and lithospheric thickness, we observe similar fault-plane orientations with depth in all three subduction zones. The dominant steep, trenchward-dipping faults of the outer rise may be reactivated down to 100 km depth, while subhorizontal faults also slip from 40-100 km depth. From 100-300 km depth, all identified faults are subhorizontal. While inconsistent with the reactivation of the dominant outer-rise fault orientation, this orientation could be consistent with the reactivation of the seaward-dipping faults, and recent numerical experiments [*Faccenda et al, 2009*] suggest that the less prominent faults may be preferentially reactivated because of the stress field in the bending slab. The similarity in the onset depth of horizontal faulting in the three subduction zones suggests that it is controlled by pressure rather than temperature or other tectonic parameters. In Tonga, which has a double seismic zone with opposite stress orientations in each plane of seismicity, deformation along these subhorizontal faults causes the slab to thin, indicating that slab pull is the primary force controlling slab seismicity at intermediate depths. While seismicity in our Middle and South America study areas stops by 250 km depth, Tonga earthquakes occur down to nearly 700 km depth. The fault-plane orientations of earthquakes >300 km depth match the patterns expected for the creation of a new system of faults: we observe both subhorizontal and subvertical fault planes consistent with a down-dip-compressional stress field. Slip along the two fault orientations causes the slab to thicken as it subducts and encounters resistance to lower mantle penetration. This resistance also results in an increase in the frequency of subhorizontal fault planes >600 km depth.

References

Warren, L.M., A.N. Hughes, and P.G. Silver (2007a), Earthquake mechanics and deformation in the Tonga-Kermadec subduction zone from fault-plane orientations of intermediate- and deep-focus earthquakes, *J. Geophys. Res., 112*.

Warren, L.M., M.A. Langstaff, and P.G. Silver (2008), Fault-plane orientations of intermediate-depth earthquakes in the Middle America trench, *J. Geophys. Res., 113*, B01304.

Warren, L.M., and P.G. Silver (2006), Measurement of differential rupture durations as constraints on the source finiteness of deep-focus earthquakes, *J. Geophys. Res., 111*.

Acknowledgements: This work was supported by the National Science Foundation through grant EAR-0733170 and through Independent Research and Development time while the author worked at the Foundation, and by the Carnegie Institution of Washington through a Harry Oscar Wood Postdoctoral Fellowship.

Automated Identification of Teleseismically Recorded Depth Phases with Application to Improving Subduction Zone Earthquake Locations

Heather R. DeShon *(CERI, Univ. of Memphis),* **E. Robert Engdahl** *(Univ. of Colorado-Boulder),* **Shishay Bisrat** *(CERI, Univ. of Memphis),* **Susan L. Bilek** *(New Mexico Institute of Technology),* **Jeremy Pesicek** *(Univ. of Wisconsin-Madison),* **Clifford H. Thurber** *(Univ. of Wisconsin-Madison)*

A large portion of the seismogenic megathrust of most subduction zones lies beneath the ocean, which ultimately limits the amount of local seismic data available for high precision earthquake location studies. Standard single-event teleseismic earthquake locations are limited in their ability to provide the level of precision necessary to properly evaluate spatio-temporal aftershock variability, to constrain subducting plate geometry, or to investigate temporal strain release. Earthquake locations in global catalogs can be in error by 10's of kilometers in location and depth due to the use of imprecise arrival time picks, phase misidentification, poor station coverage, etc. Improvements to teleseismic event location, especially in depth, can be accomplished using more accurate depth phase arrival times. We have developed a new method to identify depth phases (pP, pwP, sP) and improve P onset times that takes advantage of the high quality IRIS Global Seismic Network waveforms available through the IRIS Data Management Center. The picker uses abrupt amplitude changes of the power spectral density (PSD) function calculated at optimized frequencies for each waveform. The technique identifies depth phases not reported in the standard catalogs and works over a wide-range of depths. The additional depth phases are incorporated with the ISS, ISC, and NEIC phase catalogs and relocated using the EHB teleseismic location approach [Engdahl et al., 1998]. The automatically identified depth phases and revised EHB catalogs are being used for two subduction zone studies: 1) Teleseismic double-difference relocation and tomography along the Andaman-Sunda subduction zone, which takes advantage of the extensive global recordings of the 2004, 2005, and 2007 great (M>8) Sumatra earthquakes [i.e. Pesicek et al., 2010]; 2) A global study characterizing earthquake source durations in subduction zones, with a focus on identifying unusually slow source processes such as those associated with tsunami earthquakes [i.e. Bisrat et al., 2009]. To date, we have provided nearly 29,000 new phases to the EHB catalog for ~1250 earthquakes in the Sumatra, Java, Kurile, Japan, Peru, and Alaska subduction zones. Epicentral changes following relocation using additional depth phases are generally small (<5 km). Changes in depth may be on the order of 5-20 km for some events, while the standard deviation of depth changes within each subduction zone is ~5 km.

References

Bisrat, S.T., H.R. DeShon, E.R. Engdahl, S.L. Bilek (2009), Improved Teleseismic Locations of Shallow Subduction Zone Earthquakes, Eos Trans. AGU, 90(52), Fall Meet. Suppl., Abstract T23B-1913.

Engdahl, R.E, R. Hilst and R. Buland (1998), Global teleseismic earthquake relocation with improved travel times and procedures for depth determination. *Bull. Seismol. Soc. Amer., 88*, 722-743.

Pesicek, J.D., C.H. Thurber, H. Zhang, H.R. DeShon, and E.R. Engdahl (2010), Teleseismic Double-difference Relocation of Earthquakes along the Sumatra-Andaman Subduction Zone using a Three-Dimensional Model, *J. Geophys. Res.*, (in press).

Acknowledgements: We gratefully acknowledge NSF EAR and OCE support (EAR0608988, OCE0841022 to HRD; EAR0609613, OCE0841040 to ERE; OCE0941077 to SLB; EAR0608988 to CT).

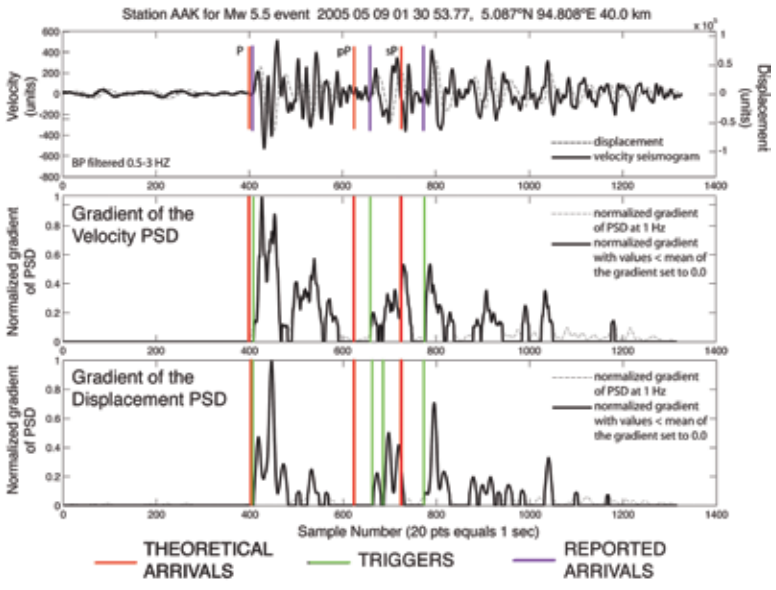

Figure 1: Example of the automated depth phase identification procedure applied to a Mw 5.5 earthquake occurring at 40 km depth in the Sunda subduction zone. (top) Velocity and displacement waveforms recorded at GSN station AAK. The theoretical arrival times for P, pP and sP (red) and the new reported arrivals (purple) following the automated procedure are shown. (middle, bottom) The automated method uses abrupt changes the gradient of the power spectral density function (PSD) of both the velocity and displacement time series, termed triggers (green), and associates triggers with likely phases. The initial identifications may be dynamically reidentified during the EHB relocation process.

The Puzzle of the Bardarbunga, Iceland Earthquake: No Volumetric Component in the Source Mechanism

Hrvoje Tkalčić *(The Australian National University),* **Douglas S. Dreger** *(University of California at Berkeley),* **Gillian R. Foulger** *(Durham University),* **Bruce R. Julian** *(United States Geological Survey)*

A volcanic earthquake with Mw=5.6 occurred beneath the Bárdarbunga caldera in Iceland on September 29, 1996. This earthquake is one of a decade-long sequence of M5+ events at Bárdarbunga with non-double-couple mechanisms in the global CMT catalogue. Fortunately, it was recorded well by the regional-scale Iceland Hotspot Project seismic experiment. We investigated the event with a complete moment tensor inversion method [*Tkalčić et al., 2009*] using regional long-period seismic waveforms and a composite structural one-dimensional model from receiver function and surface wave constraints. The moment tensor inversion using data from stations of the Iceland Hotspot Project yields a non-double-couple solution with a 67% vertically oriented compensated linear vector dipole component, a 32% double-couple component and a statistically insignificant (2%) volumetric (isotropic) contraction. This indicates the absence of a net volumetric component, which is puzzling in the case of a large volcanic earthquake that apparently is not explained by shear slip on a planar fault. A possible volcanic mechanism that can produce an earthquake without a volumetric component involves two offset sources with similar but opposite volume changes. We show that although such a model cannot be ruled out, the circumstances under which it could happen are rare.

References

Tkalčić H., D. S. Dreger, G. R. Foulger, and B. R. Julian (2009). The puzzle of the Bardarbunga, Iceland earthquake: No volumetric component in the source mechanism, *Bull. Seismol. Soc. Amer., 99*: 3077-3085.

Acknowledgements: We are grateful to IRIS DMC center for efficiently archiving and distributing continuous waveform data.

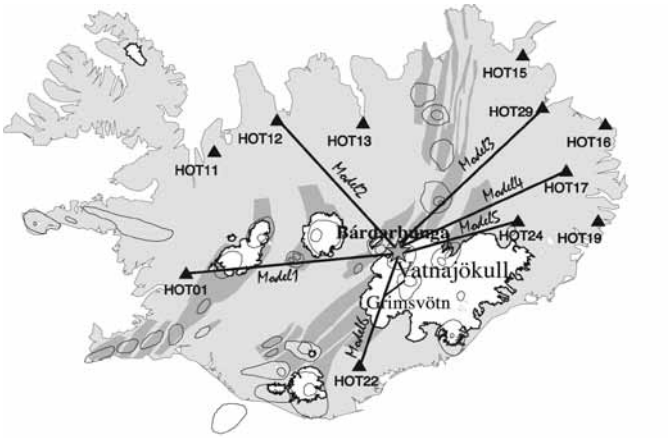

Figure 1

Map showing the main tectonic and volcanic features in Iceland. Glaciers are shown in white and spreading segments in dark gray. Volcanoes are shown with thin lines. The Bárdarbunga earthquake is shown with the white star. Triangles are locations of the eleven Iceland Hotspot Project broadband stations used in the moment tensor inversion. Lines indicate the locations of the six different one-dimensional models used between the source and stations.

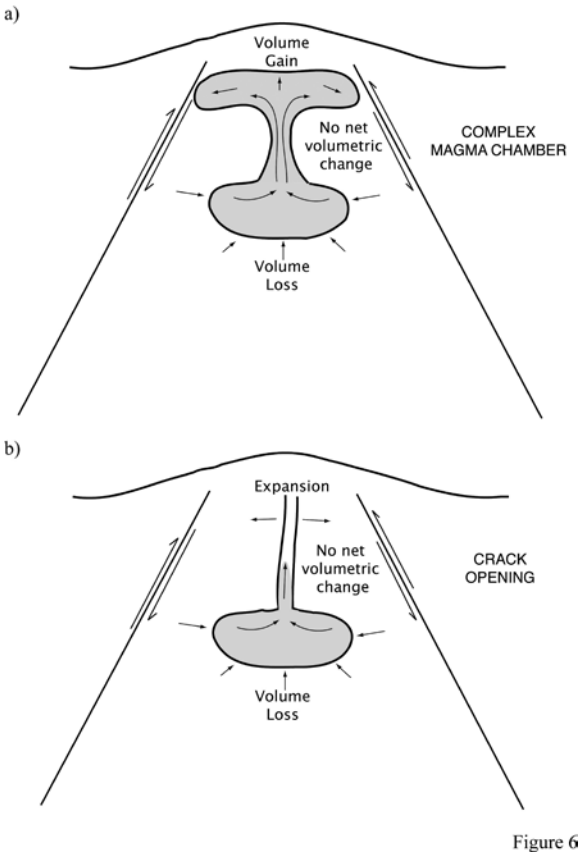

Figure 6

Sketch of tested models with two compensating sources reproducing a vertically oriented CLVD in dilatation (where volumetric exchange is equal and opposite in sign): (a) a complex magma chamber; (b) an implosive source and a vertical, horizontally opening crack above.

Evaluating Ground Motion Predictions of Usgs 3d Seismic Model of the San Francisco Bay Area with Broadband Seismograms

Arthur Rodgers *(Lawrence Livermore National Laboratory),* **Anders Petersson** *(Lawrence Livermore National Laboratory)*

The USGS (Menlo Park) developed a three-dimensional (3D) geologic and seismic model of the greater San Francisco Bay Area for the purposes of computing earthquake ground motions. This model was used to compute scenario ground motions for the 1906 San Francisco [Aagaard et al., 2008b], 1989 Loma Prieta [Aagaard et al., 2008a] and a suite of Hayward Fault earthquakes [Aagaard et al., in press]. While scenario ground motion calculations are important for investigating the amplitude, duration and variability of motions from large damaging earthquakes, the accuracy of such predictions depends on the accuracy of the 3D model. We evaluated the USGS 3D model of the Bay Area by computing predictions of broadband waveforms for 12 moderate (Mw 4-5) earthquakes and comparing them to the observed waveforms [Rodgers et al., 2008]. Calculations were performed using WPP (an elastic finite difference code developed at LLNL) on massively parallel computers. Data were obtained from IRIS for Berkeley Digital Seismic Network (BDSN) and USArray broadband stations. The figure below shows a snapshot of the vertical component displacements for an earthquake near Glen Ellen (Sonoma County). Also shown is the comparison of the observed (blue) and computed (red) three-component seismograms at two stations: BKS (Berkeley) and JRSC (Stanford). Note that the motions at BKS are more complex and longer duration due to basin propagation effects from the San Pablo Bay, however the 3D model predicts this energy quite well. The motions at JRSC are simpler and the 3D model predicts the weaker late arriving energy on the transverse (T) component. This analysis found that the USGS 3D model could predict the amplitude, duration and waveform shapes of moderate earthquake ground motions quite well however we did find that phase delays reveal that shear velocities in the model were too fast. This information was used to revise the model for subsequent ground motion modeling.

References

Aagaard, B., T. Brocher, D. Dreger, A. Frankel, R. Graves, S. Harmsen, S. Larsen, K. McCandless, S. Nilsson, N. A. Petersson, A. Rodgers, B. Sjogreen and M. L. Zoback, (2008b). Ground motion modeling of the 1906 San Francisco earthquake II: Ground motion estimates for the 1906 earthquake and scenario events, *Bull. Seismol. Soc. Amer., 98*, 1012-1046

Rodgers, A., A. Petersson, S. Nilsson, B. Sjogreen and K. McCandless (2008). Broadband Waveform Modeling of Moderate Earthquakes in the San Francisco Bay Area To Evaluate the USGS 3D Seismic Velocity Model, *Bull. Seismol. Soc. Amer., 98*, 969-988

Acknowledgements: This work performed under the auspices of the U.S. Department of Energy by Lawrence Livermore Nation

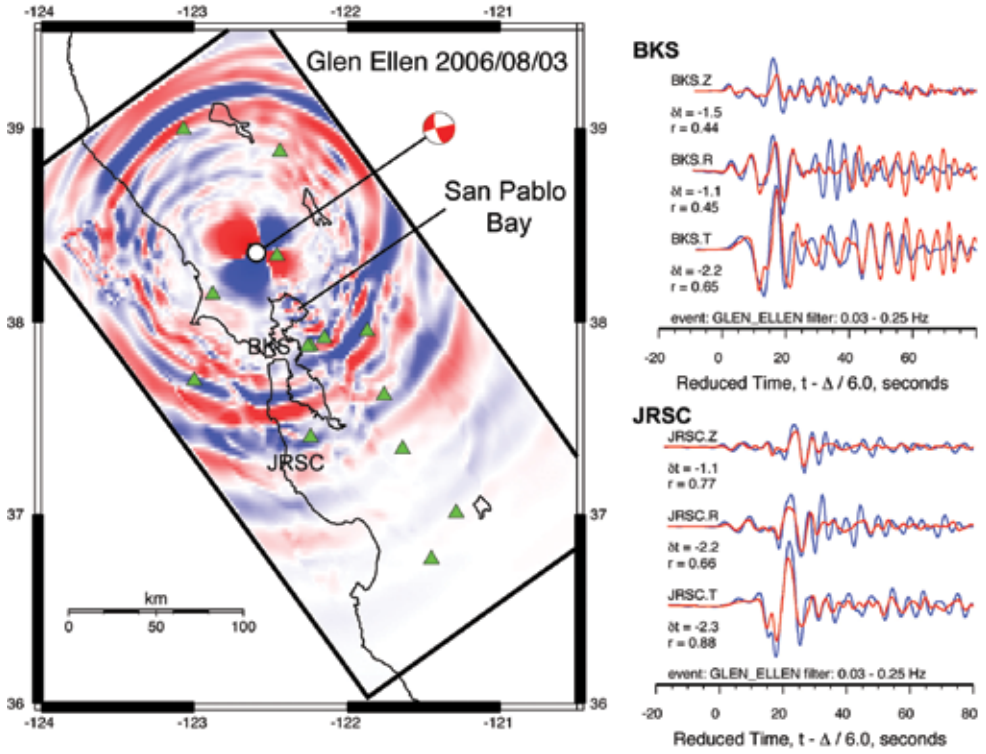

(left) Snapshot of vertical component displacement for an earthquake near Glen Ellen with BDSN and USArray broadband stations (green triangles). (right) Comparison of observed (blue) and computed (red) three-component seismograms at stations BKS (Berkeley, top) and JRSC (Stanford, bottom).

Physics-Based Shake Map Simulation for the 2008 Wells, Nevada Earthquake

John N. Louie *(University of Nevada, Reno)*

The standard USGS ShakeMap for the Feb. 21, 2008 M6.0 Wells, Nevada earthquake shows many "bulls-eye" anomalies. The simple ShakeMap algorithm tried to average between high shaking in the populated basins reported by citizens to the USGS Community Internet Intensity Map (CIIM), and low shaking measured at several USArray Transportable Array (TA) stations on bedrock. Starting with the complex basin-thickness map of Saltus and Jachens [1995], we built a 3d seismic-velocity model that also included a projection of shallow geotechnical velocities. Various models for the directivity of rupture of 15x15-km normal-fault planes fed into computations predicting shaking across the region, employing the physics-based E3D code of Larsen et al. [2001]. The simulated peak-ground-velocity (PGV) maps show a high degree of channeling along the many basins in the region, with adjacent basin and bedrock areas only 2 km apart predicted to experience levels of shaking differing by a factor of ten. There is also evidence that strong basin shaking "tunnels" across narrow parts of bedrock ranges separating basins. The physics-based shake map is highly heterogeneous in this Basin and Range region (see figure) and contains prominent features that a standard, statistical USGS ShakeMap cannot predict. The physics-based simulation produces a good match against PGV values recorded at nearby TA stations, when an eastward rupture directivity is used at the source. The match is highly sensitive to the rupture directivity.

References

Larsen, S., Wiley, R., Roberts, P., and House, L., 2001, Next-generation numerical modeling: incorporating elasticity, anisotropy and attenuation: Society of Exploration Geophysicists Annual International Meeting, Expanded Abstracts, 1218-1221.

Saltus, R. W., and Jachens, R. C., 1995, Gravity and basin-depth maps of the Basin and Range Province, Western United States: U.S. Geological Survey, Geophysical Investigations Map, Report: GP-1012, 1 sheet.

Acknowledgements: Research partially supported by the U.S. Geological Survey (USGS), Department of the Interior, under USGS award numbers 08HQGR0046 and 08HQGR0015. The views and conclusions contained in this document are those of the authors and should not be interpreted as necessarily representing the official policies, either expressed or implied, of the U.S. Government.

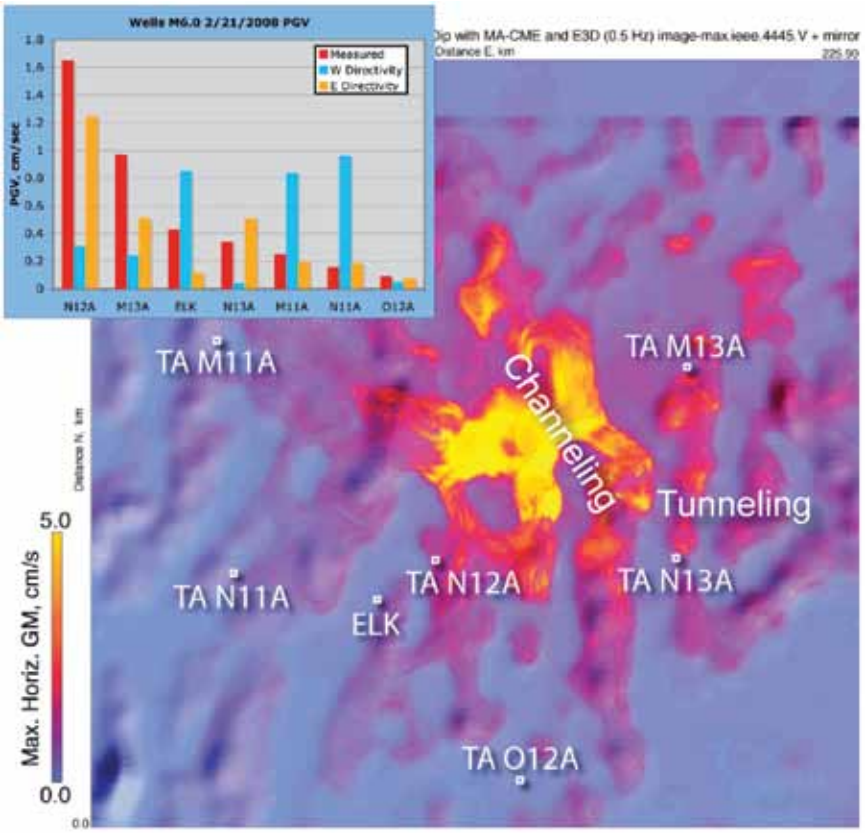

Shaded-relief map of basin-floor topography in northeastern Nevada (Saltus and Jachens, 1995) surrounding the Feb. 21, 2008 Wells earthquake, 225 km on a side (the basin dataset used ends artificially at 42°N). Locations of USArray Transportable Array (TA) stations recording the event are indicated. Warmer colors correspond to greater shaking computed for the event by the E3D code of Larsen et al. (2001), including the effects of geologic basins and predicted geotechnical velocities. Solid yellow indicates peak ground velocities (PGV) above 5 cm/s. This computation assumes an eastward directivity of the earthquake rupture. Shaking is high along the many basins, and high levels of shaking channel along the basins and can tunnel across ranges between basins, with examples indicated. In the inset graph this shaking prediction (orange bars) matches the recorded PGV (red) well, while other directions of directivity (blue) do not match.